Erosion Behavior of Sand-Silt Mixtures
Revisiting the Erosion Threshold

Yao, Peng; Su, Min; Wang, Zhengbing; van Rijn, Leo C.; Stive, Marcel J.F.; Xu, Chunyang; Chen, Yongping

Important note
To cite this publication, please use the final published version (if applicable).
Please check the document version above.

Water Resources Research®

RESEARCH ARTICLE

10.1029/2021WR031788

Key Points:

- Silt content is an important factor controlling the erosion of sand-silt mixtures in regards to noncohesive or cohesive properties
- There exists a critical silt content of 35%, beyond which a stable silt skeleton is formed that increases the erosion threshold
- A modified critical bed shear stress is proposed to mimic the transitional erosion behavior of sand-silt mixtures

Erosion Behavior of Sand-Silt Mixtures: Revisiting the Erosion Threshold

Peng Yao[1,2,3] , Min Su[2,4,5] , Zhengbing Wang[6,7] , Leo C. van Rijn[8], Marcel J. F. Stive[6] , Chunyang Xu[2], and Yongping Chen[1,2]

[1]State Key Laboratory of Hydrology-Water Resources and Hydraulic Engineering, Hohai University, Nanjing, China, [2]College of Harbour, Coastal and Offshore Engineering, Hohai University, Nanjing, China, [3]State Key Laboratory of Coastal and Offshore Engineering, Dalian University of Technology, Dalian, China, [4]Jiangsu Key Laboratory of Coast Ocean Resources Development and Environment Security, Hohai University, Nanjing, China, [5]State Key Laboratory of Estuarine and Coastal Research, East China Normal University, Shanghai, China, [6]Faculty of Civil Engineering and Geosciences, Delft University of Technology, Delft, The Netherlands, [7]Deltares, Delft, The Netherlands, [8]LVR-Sediment Consultancy, Blokzijl, The Netherlands

Abstract The erosion threshold, beyond which bed sediments start to move, is a key parameter describing sediment transport processes. For silt-dominated mixtures, in which the grain size is between sand and clay, existing experimental studies exhibit contradictory observations. That is, the erosion was either sand-like or clay-like, suggesting transitional erosion behavior. To explore the underlying mechanism of the transitional erosion behavior of silt-sized sediment, we revisited the topic of the erosion threshold of sand-silt mixtures by carrying out a series of erosion experiments for different bed compositions. The results suggest that there exists a critical silt content of approximately 35%, separating two domains. Below this critical value, the critical bed shear stress follows the Shields criterion, whereas above this value, the erosion threshold of a mixed bed increases abruptly and remains relatively constant with a further increase in silt content. By combining with existing data, we found that the proposed critical silt content acts as a tipping point, beyond which the mixed bed shifts from a sand-dominated to a silt-dominated domain. For the silt-dominated domain, a stable silt skeleton can be formed by attraction forces that resist erosion. However, the attraction forces are too weak to form a stable silt skeleton when the silt content is too small. Based on this finding, a modified critical bed shear stress formula is proposed for silt-dominated mixtures, which results in a better agreement with experimental data (an averaged bias of 10%), performing better than existing formulas (larger than 30%).

Plain Language Summary When exposed to a certain flow velocity, sediment particles are dislodged from the seabed, namely, the erosion threshold. Attributed to sizes, shapes, minerals, etc., sediments of different grain sizes behave differently, resulting in various erosion behaviors. Sand particles (62.5–2,000 μm) are not sticky and erode particle by particle, whereas clay particles (<4 μm) are sticky and collectively erode as chunks. Silt (4–62.5 μm), of which the grain size is between sand and clay, exhibits either sand-like or clay-like behavior, suggesting transitional erosion behavior. Coastal sediments are usually mixtures of clay, silt, and fine sand. Different bed compositions result in different erosion behaviors, leading to a variety of bed forms, morphological patterns, etc. Therefore, a thorough understanding of the erosion behavior of sediment mixtures is of great significance to the topic of coastal sediment transport, which further benefits coastal geomorphology, ecology, etc. This study indicates that, for sand-silt mixtures, a critical silt contents exists, beyond which the bed mixtures shift from a sand-like erosion behavior to a clay-like erosion behavior. The widely adopted parameterized expression of the erosion threshold (namely, the Shields curve) is modified to mimic the transitional erosion behavior of sand-silt mixtures by considering the effects of silt content.

1. Introduction

Coastal sediments are usually mixtures of particles of various sizes, such as clay (<4 μm), silt (4–62.5 μm) and fine sand (62.5–500 μm), as well as organic matter (van Rijn, 2006). Classification of sediment fraction is defined by sediment size according to the Wentworth grain size scale. Sand- or sand-dominated mixtures are noncohesive and eroded particle by particle, whereas clay-dominated mixtures are cohesive and have a strong relationship between particles. Silt or silt-dominated mixtures with limited clay content, which are widely distributed in the Modern Yellow River Delta (Jia et al., 2020), Jiangsu coast (C. K. Zhang, 2012), etc., have been proven to hold

the dual features of both sand and clay (Lamb & Parsons, 2005; te Slaa et al., 2013; Yao et al., 2015). Since coastal sediment transport is significantly dependent on bed compositions, it is important to understand the dynamic behavior of both individual sediment species and mixed sediment, as this behaviour influences coastal sedimentology, geomorphology, ecology, etc (Baar et al., 2019; Buscombe & Conley, 2012; Fagherazzi et al., 2012; Greenwood & Xu, 2001).

Erosion threshold (i.e., critical bed shear stress), beyond which sediment is initiated into motion, is an important parameter describing sediment transport. Over the decades, considerable effort has been made to understand the erosion threshold of sediment grains of various sizes. For uniform sand mixtures, a widely adopted erosion standard is the Shields curve and its subsequent revisions (Dou, 2000; Miller et al., 1977; Soulsby, 1997; van Rijn, 2007a). The Shields curve was determined experimentally by observing the erosion of particles of different sizes and densities in flows with different bed shear stresses. This curve was subsequently explained on the basis of the balance of forces (moment) acting on a single particle (Shields, 1936; van Rijn, 1993). For nonuniformly graded sandy mixtures, the Shields curve is also applicable when introducing extra parameters, such as the hiding and exposing factor (Buscombe & Conley, 2012; Kleinhans & van Rijn, 2002; van Rijn, 2007b). Mud (composed of clay and silt) is usually cohesive (depending on clay content) and collectively eroded as chunks due to electrochemical effects. Several erosion modes with different thresholds have been identified (Winterwerp & van Kesteren, 2004; M. Zhang & Yu, 2017). Generally, the erosion threshold of both sand and clay refers to the collective motion of bed materials rather than single particles.

For mixtures composed of both cohesive and noncohesive sediments, the clay content (i.e., <4 μm) is found to be the key parameter controlling erosion behavior. The mixture behaves as cohesive sediment when the clay content is larger than 5%–10% (van Ledden et al., 2004). Meanwhile, the network structure (i.e., packing status) of sediment grains also plays a role in erosion behavior (van Ledden et al., 2004). Based on ample experimental data sets of bed materials such as sand, mud, and sand-mud (e.g., Jacobs et al., 2011; Panagiotopoulos et al., 1997), recent studies have focused on summarizing unified formulas for the erosion threshold of sediment mixtures, and many achievements have been made (Dou, 2000; van Rijn, 2007a, 2020; Wu et al., 2018). Although the formulas derived from these studies are different in form, they basically treat the mud fraction (i.e., <62.5 μm) as cohesive (i.e., clay-dominated mud) and divide the sediment mixtures into sand and mud fractions, aiming to correct the original Shields curve by proposing a series of parameters with consideration of the mud content.

As mentioned above, cohesive sediment usually refers to mixtures with a certain clay content (at least larger than the critical clay content for cohesion, i.e., 5%–10%). On the other hand, silt- or silt-dominated mixtures with limited clay content have been shown to behave differently from both sand- and clay-dominated mixtures. For example, previous erosion tests suggested that silty beds can hardly be eroded and exhibit cohesive-like behavior (Roberts et al., 1998), but flocculation has not been observed in suspended silt (te Slaa et al., 2013, 2015). Rippled bed forms were observed instead of fluid mud under waves (Lamb & Parsons, 2005; Yao et al., 2015). Therefore, the existing formulas deduced from clay-dominated mud are not yet applicable for silt-sized sediment. Silt-sized sediment should be treated as a stand-alone species and requires in-depth study to understand its erosion behavior. This will improve existing erosion theories on sand-silt mixtures and is important for understanding sediment transport over silt-dominated systems (e.g., the Modern Yellow River Delta, Jiangsu coast).

White (1970) is probably the first researcher studying the erosion threshold of silt in both freshwater and oil, which represent different fluid viscosities. Based on the results of White (1970), Miller et al. (1977) found that the erosion threshold of silt satisfactorily fits a modified Shields curve of noncohesive sand. However, Roberts et al. (1998) demonstrated that the erosion threshold of quartz silt-sized sediment is several times larger than that derived from the Shields curve. Erosion tests of Roberts et al. (1998) further showed that silts with sizes smaller than <40 μm were eroded as chunks behaving as cohesive sediment. On the one hand, such opposite experimental results may be caused by differences in experimental settings, for example, the preparation of sediment bed. On the other hand, these controversial results also imply a transition behavior of silt-dominated mixtures from noncohesive to cohesive. The grain size distribution, network structure, and near-bed flow may influence the erosion threshold of silt or sand-silt mixtures. Bartzke et al. (2013) and Bartzke and Huhn (2015) proposed a conceptual model of a pore-space-filling network for a bimodal sand-silt bed. The pore space is reduced with an increase in silts exerting a blocking effect on porewater flow, resulting in bed stabilization. Mohr et al. (2018) suggested that permeability could be a useful metric to predict the erosion threshold as well as the erosion rate of marine unimodal sandy mixtures. Staudt et al. (2017, 2019) investigated the effects of the grain size distribution

Table 1
Representative Parameters of the Bed Materials Used in This Study

Exp Nr.	D_{10} (μm)	D_{50} (μm)	D_{90} (μm)	D_{90}/D_{10}	P_{clay} % (<8 μm)	P_{silt} % (8–62.5 μm)	P_{sand} % (>62.5 μm)	$D_{50,silt}$ (μm)	$D_{50,sand}$ (μm)	RD
E79	22	43	71	3	3	79	18	39	73	2
E66	26	50	84	3	3	66	31	43	77	2
E60	24	52	99	4	4	60	36	41	83	2
E49	24	60	111	5	4	49	47	42	88	2
E36	21	72	136	6	5	36	59	42	98	2
E29	42	81	137	3	1	29	70	48	96	2
E19	50	96	172	3	1	19	80	50	109	2

Note. Clay fraction (P_{clay}) herein refers to sediment grains whose sizes are smaller than 8 μm. RD is the ratio of coarse grains to fines, and $RD = D_{50,sand}/D_{50,silt}$.

on the erosion threshold of various bimodal sandy beds. These researchers reported that the grain-size ratio (RD) between coarse and fine grain sediment controls whether the bed is stabilized or mobilized by the existence of fines by influencing the bed roughness, near-bed flow and network structure. Regarding natural silt-dominated coastal systems, which are usually composed of unimodal silt-sized sediment mixtures, whether the existing theories can be applied to the transition behavior of silts is still unclear.

The main objective of this study is to understand the abovementioned erosion behavior (i.e., transitional behavior) of silt-dominated mixtures and explore the underlying mechanisms for controlling the transition from noncohesive to cohesive behavior of silt. To this end, a series of erosion experiments was carried out for silt-dominated mixtures with various sediment compositions using an annular flume. The erosion threshold was deduced based on near-bed turbulence. Furthermore, bed configurations, near-bed flow regimes and microstructures of different sediment mixtures were compared and analyzed. Based on these analyses, we attempted to find the tipping point of the silt transition behavior and explore the underlying mechanisms. Finally, an effort was made to parameterize the erosion threshold for practical and modeling purposes in silt-dominated systems.

2. Materials and Methods

2.1. Bed Materials

Bed materials were collected from the Tiaozini tidal flat at the central Jiangsu coast, China, as described in Yao et al. (2015). Originally, two types of sediment mixtures were distinguished: a silt-enriched mixture with a median grain size of 46 μm and a very fine sand-enriched mixture with a median grain size of 88 μm. Based on bed sample surveys in silt-dominated systems, the silt content at the Jiangsu coast ranges from 10% to 80% (Kuai et al., 2021) and 48%–85% at the Modern Yellow River Delta (Jia et al., 2020). Therefore, the collected sediment samples were first separated into several different sediment fractions and then remixed into seven groups of sand-silt mixtures with different compositions to cover the field variations. The separation was carried out in a transparent bucket with a rotating paddle in the middle. Since the settling velocities are different for sediment grains of different sizes, different sediment fractions can be separated by changing the rotating speed of the paddle. The grain size distribution of the bed materials used in this study was measured by a Malvern Mastersize 3,000 laser particle size analyzer (see Figure S1 in Supporting Information S1). Table 1 presents several parameters of sediment bed composition. Each sediment mixture is named by the percentage of the silt content after the letter "E". Van Rijn (2006, 2020) and Yao et al. (2015) suggested that the cohesion of mixtures is mainly attributed to the content of clay and the very fine silt fraction (<8 μm). Therefore, to concentrate on the erosion behavior of silt-sized sediment only, sediment grains with sizes smaller than 8 μm were kept as low as possible (i.e., <5%) to exclude the cohesive effect. Table 1 shows that the silt content varies from 19% to 79%, covering most bed compositions in silt-dominated systems. Note that we only changed the silt contents of the sediment mixtures. The properties of sediment mixture, such as dry bulk density and permeability, may change with different silt contents. Therefore, the bed properties were also measured and are discussed.

Table 2
*Bed Properties of Different Sand-Silt Mixtures in This Study*

Exp. Nr.	D_{50} (μm)	P_{silt} (%)	Initial ρ_{dry} ($\times 10^3$ kg/m^3)	ρ_{dry} after 1 hr ($\times 10^3$ kg/m^3)	Max. ρ_{dry} ($\times 10^3$ kg/m^3)	Min. ρ_{dry} ($\times 10^3$ kg/m^3)	k (m/s)
E79	43	79	1.29	1.41	-	-	2.17×10^{-06}
E66	50	66	1.30	1.39	1.51	1.15	2.51×10^{-06}
E60	52	60	1.29	1.39	1.51	1.18	2.34×10^{-06}
E49	60	49	1.37	1.44	1.50	1.19	2.32×10^{-06}
E36	72	36	1.33	1.43	1.52	1.17	2.05×10^{-06}
E29	82	29	1.63	1.66	-	-	4.17×10^{-06}
E19	96	19	1.62	1.67	-	-	4.90×10^{-06}

Note. ρ_{dry} is the dry bulk density. k refers to permeability. k was measured at a fixed dry bulk density of 1,500 kg/m^3.

The sand-silt mixtures were first mixed with a certain amount of tap water for the preparation of a saturated sediment bed in the annular flume. Subsequently, the whole flume was covered with a flat sediment bed with a thickness of ∼2.5 cm. The prepared sediment bed was allowed a certain time (∼120 min) to compact. Note that the salinity of coastal waters may affect the properties of fine-grained sediments, especially clay minerals. Lick and McNeil (2001) suggested that the effect of gelation plays a major role in the erosion threshold of clay minerals (e.g., bentonite). A high salinity may decrease the erosion threshold of bentonite, while for silt-sized sediment, the difference in erosion thresholds under salt water and clean water is relatively small. In a parallel study on settling processes of silt-dominated sediment, we find that in salt water (2%–35% salinity), no flocculation can be observed for silt grains larger than 40 μm, while weak flocculation can be detected for grains ranging between 8 and 40 μm (Yao et al., 2022). The salinity is proposed to have a limited effect on the erosion threshold of silt-dominated mixtures. Therefore, all experiments in this study were conducted under freshwater condition. Future work will consider saltwater conditions. Before each experiment, the flume was cleaned, and the sediment bed was reprepared to ensure the consistency of the bed compositions.

To ensure similar bed configurations (i.e., dry bulk densities, porosities, etc.) for different groups of erosion experiments, a preliminary compaction experiment was conducted first. A 2.5 cm thick sediment bed (same thickness as in the annular flume) was prepared in a transparent and scaled glass column. Then, tap water was slowly added to the column to an elevation of 30 cm (same water depth in the erosion experiment) above the sediment bed. The height of the surface sediment bed and the volume of the sediment bed were regularly recorded. The dry bulk density of the mixtures increased rapidly in the first 60 min and then approached a relatively stable value (see Figure S2 in Supporting Information S1, taking sediment mixture E66 as an example). This indicates that the silt-sized sediment bed was compacted in a relatively short time period (∼60 min) under self-weight and freshwater conditions. Based on the results of this compaction experiment, the sediment beds of all groups of experiments in the annular flume were first compacted for 2 hr in 30 cm deep water before the onset of flow.

Bed properties, such as maximum and minimum dry bulk densities and permeabilities of different sand-silt mixtures, were measured by standard geotechnical test procedures (at the geotechnical center of Hohai University), as listed in Table 2. Initial dry bulk density and that after 1 hr, which were measured during experiments, were compared with the maximum and minimum values. Consistent with the aforementioned compaction experiments, the results indicate that the initial silty beds can reach 90% of their maximum bulk density in 1 hr. This rapid compaction feature of the silty bed is similar to that of a noncohesive sandy bed, in accordance with the study of te Slaa et al. (2013). Thus, in erosion experiments, a deposition time of 2 hr before the introduction of flow is sufficient for the initial bed density toward its stable value, suggesting sand-like behavior. Since the dry bulk density of silty beds (i.e., sediment mixtures E36-E79) were more or less the same after 1 hr, the permeabilities of different mixtures were measured at a fixed dry bulk density (i.e., 1,500 kg/m^3) for all samples following a variable head permeability test procedure.

Water Resources Research
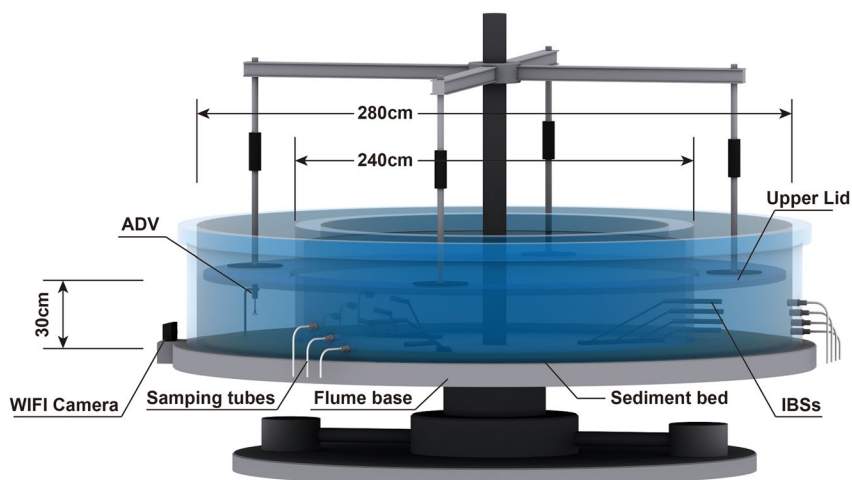
Figure 1. Overview of the annular flume and setup of instruments.

2.2. Annular Flume Experiment Setup

Erosion experiments were carried out in the annular flume at Hohai University, China, following a setup similar to Yao et al. (2018). The annular flume has an outer diameter of 2.8 m and an inner diameter of 2.4 m (Figure 1). The width of the flume is 0.2 m. A rotating lid was placed on top of the flume, by which the water depth (0.3 m in this study) can be adjusted. The lid and the flume base can be rotated in opposite directions simultaneously to minimize secondary flows associated with curvature (as described in Booij, 1994). The optimum rotation rate ratio between the lid and flume base was precalibrated. By increasing the rotation of the lid and flume base, different levels of flow velocities can be generated inside the flume.

The flume was equipped with a Nortek *ADV* (Vectrino Profiler II) in the middle, by which a 3D velocity profile of a 35 mm-thick layer above the sediment bed was recorded (Figure 1). The near-bed velocity profile is measured with an interval of 1 mm vertically and a sampling frequency of 25 Hz. The *ADV*, with boundary detection functionality, was applied to record bed level changes with a sampling frequency of 1 Hz. Preliminary tests showed that the water-sediment interface detected by the *ADV* is several millimeters below the "real" sediment bed surface. This is because the *ADV* only recognizes the bins with the strongest acoustic backscatter as a solid boundary, as mentioned in Staudt et al. (2017). This *ADV* deviation can be corrected by manually measuring the height of the sediment bed at the beginning of the experiment (and each velocity level). Note that boundary detection is only applicable at low sediment concentrations. When the near-bottom concentration was larger than 5 kg/m³ (i.e., in this study), the *ADV* failed to obtain correct bed boundaries.

Nine infrared backscatter sensors (*IBSs*, designed and manufactured by the experimental center of Hohai University, see Wang et al., 2007), which are similar to commonly used optical backscatter sensors but with smaller sensor sizes (diameter of ∼5 mm), were firmly installed on and penetrated the inner wall, following the curvature of the flume (Figure 1). These *IBS*s were grouped into three sections distributed in different places of the annular flume and at different elevations to monitor suspended sediment concentration (*SSC*) changes during experiments. The elevations of the *IBS*s were 1.60, 5.45, and 11.70 cm (Section 1), 1.85, 7.25, and 14.10 cm (Section 2), and 3.40, 9.70, and 15.55 cm (Section 3) above the actual flume bottom. Note that several sensors may be submerged in the 2.5 cm thick sediment bed. *IBS*s can provide real-time electrosignals (i.e., voltages), which is beneficial for detecting the erosion threshold (see Section 2.3.2 for details). At the same height but at the opposite sides of the flume, there are several corresponding openings connected with rubber tubes, by which water-sediment mixtures can be sampled for signal calibration. The calibration procedures for conversion of *IBS* signals to *SSC*s follow Su et al. (2016). See Figure S3 in Supporting Information S1 for more information on *IBS* calibration. The *SSC*s measured by this system were used to determine the erosion threshold using the methods described below.

To visually monitor the erosion behavior of different groups of sand-silt mixtures, a video detection system was designed composed of two individual cameras. One camera is WIFI-based and installed on the outer wall of the

Table 3
Near-Bed Velocity (at z = 2 cmab) at Each Velocity Level Under Freshwater Conditions

Velocity levels	1	2	3	4	5	6	7
Velocity magnitude (m/s)	0.04	0.09	0.14	0.18	0.21	0.26	0.35

flume (Figure 1). It can be rotated with the flume base, and the high-resolution videos recording sediment bed erosion can be remotely accessed by a smartphone. Subsequently, bed erosion behavior (i.e., particle erosion and bed forms) can be recorded visually during the experiment. The other camera was placed at a distance (∼2 m) away from the flume, and it did not rotate with the flume so that the side projection of the whole annular flume could be captured. Long-exposure photography (8 s of exposure time) was adopted to record water color during each level of the flow velocity (see Figure S4 in Supporting Information S1) by the second camera. This camera mainly served as an assistant tool for a preliminary judgment of the initiation of erosion, rather than measuring the variation in *SSC*.

All experiments started from clean water, zero velocity and a flat sediment bed condition. The upper lid and the flume base were individually increased to the desired rotation speeds in a short time span. When a stable *IBS* signal was achieved, the water-sediment mixtures were sampled. Subsequently, the next velocity level was applied by altering the precalibrated rotation speed of the annular flume. In total, 10 discrete velocity levels were calibrated. Since the present study focused on the erosion threshold of the sand-silt mixtures, only the first seven velocity levels were analyzed. Since the near-bed flow velocity varies with different bed mixtures, the velocity of fresh water experiment over a fixed bed was used as a reference listed in Table 3, which was measured at 2 cm above the bed (hereinafter referred to 2 cmab). Each group of experiments utilized the same rotation speed of the flume and was repeated twice or four times (depending on the consistency of observations during experiments) to ensure repeatability. An error analysis (mainly for critical bed shear stress) of experiments was performed with more than three repetitions. See Section 3.5 for details.

2.3. Data Processing

2.3.1. Bed Shear Stress Estimation

The velocity data measured by the *ADV* were used to calculate the near-bottom turbulence and then to estimate the bed shear stress. The velocity data were first filtered to remove the poor-quality data (beam correlations <70% and signal-to-noise ratios <12). Next, these filtered data were despiked by the phase-space threshold method (Goring & Nikora, 2002). The velocity data over the last 5 min at each velocity level were extracted to calculate the bed shear stress using the turbulent kinetic energy (*TKE*) approach, which has been suggested to be the best option for annular flumes by previous studies (e.g., Kim et al., 2000; Pope et al., 2006; Staudt et al., 2017). The *TKE* was calculated by:

$$TKE = \frac{1}{2}\rho_{\mathrm{w}} \left(\overline{u_x'^2} + \overline{u_y'^2} + \overline{u_z'^2} \right) \tag{1}$$

where *TKE* (N/m^2) is the turbulence kinetic energy, ρ_w is the water density, and u_x', u_y', and u_z' are the velocity fluctuations in the along-channel, cross-channel and vertical directions, respectively. It is recommended that the representative *TKE* for calculating the bed shear stress should be taken within the flow boundary layer and at the elevation where the *SNR* (i.e., signal-to-noise ratio) is the highest and the reliability of the measurement is the greatest (Pope et al., 2006). The annular flume has a confined boundary layer, and the typical boundary layer thickness in this study is ∼2.7 cm (see the velocity profile in Section 3.4 for details). The SNR reaches its peak at an elevation of 2.5 cm above the sediment bed. Thus, the representative *TKE* of all experiments was calculated at an elevation of 2.5 cmab. It is noted that because of scale differences between different annular flumes, the elevation for the *TKE* calculation varies. The bed shear stress τ_b is estimated by the representative *TKE* through $\tau_b = C_1 \cdot TKE$. C_1 is a constant and is set as 0.19 for the annular flume (Pope et al., 2006). Statistical analysis shows that a slight vertical shift (∼3 mm) relative to the representative measuring elevation (2.5 cm) can result in a 10% change in *TKE*, leading to a variation in the critical bed shear of ∼0.02 Pa.

There are many methods to estimate bed shear stress from *ADV* measurements in addition to the *TKE* method, such as the log profile method (*LP*) and the Reynolds stress method (i.e., the direct covariance method, *COV*). Many existing studies have focused on the applicability and accuracy of these methods. Regarding erosion experiments in the annular flume, the *COV* method can result in erroneous estimates of bed shear stress due to the existence of secondary flow and tilting of the *ADV* (Pope et al., 2006). The *LP* method is sensitive to variations in bed level. The *TKE* method is concluded to be the most robust method for estimating bed shear stress (Pope et al., 2006). In this study, we also compared these methods and the conclusion is consistent with previous studies, such as Kim et al. (2000) and Pope et al. (2006).

2.3.2. Identification of the Erosion Threshold

For noncohesive sandy grains, the erosion threshold may be visually judged according to four stages of incipient motion defined by Kramer (1935). However, Kramer's visual distinction can hardly apply to fine-grained mixtures (Panagiotopoulos et al., 1997). The erosion threshold of fine-grained sediment is commonly estimated by using either a critical erosion rate or a critical *SSC* (e.g., Mohr et al., 2018; Roberts et al., 1998; Staudt et al., 2017). However, definitions of either critical erosion rate or critical *SSC* vary significantly in different studies (Amos et al., 1997). For example, the critical erosion rate was $\sim 10^{-4}$ cm/s in work by Roberts et al. (1998) and $\sim 10^{-5}$ cm/s in Mohr et al. (2018). Thus, the results of existing studies suggest that there is no uniform value of either the critical erosion rate or *SSC* to determine the erosion threshold (Sutherland et al., 1998).

In this study, the erosion threshold was determined according to the following procedures. First, the *SSC* was used as an indicator for the erosion threshold. For the experiment with a coarse sediment bed (i.e., sediment mixture E19), the critical value of the *SSC* was found to be 0.04 kg/m³ (at the level of ~ 2.9 cmab), which provides a bed shear stress of 0.097 Pa. This value is comparable to that calculated by the Shields curve (0.10 Pa). Then, this critical *SSC* was used as a unified criterion to deduce the critical bed shear stress in all experiments. Second, the bed erosion behavior monitored visually by cameras was considered to verify the deduced erosion threshold in the first step. The proposed camera system records both water color variations (recorded by an overall camera, see Figure S4 in Supporting Information S1) and local bed form conditions (recorded by a local camera, see Figure 2). Since the onset of bed erosion not only changes *SSC*s but also alters the bed level, by integrating the abovementioned procedures, the erosion threshold can be identified.

3. Results

3.1. Overall Erosion Behavior

Figure 2 depicts close-up photographs near the sediment bed taken by a WIFI camera at different velocities and for different sediment beds. By adjusting the angle of the camera lens, both the surface and side of the sediment bed can be captured. Time-averaged *SSC*s (measured by *IBSs*) are also labeled. For all experimental groups, with increasing flow velocity, the water color gradually became turbid, and *SSC*s increased as well. The bed surface remained flat at velocity levels 1–6 and then developed into a rippled bed at velocity level 7, except for sediment mixture E60 (with $\sim 60\%$ silt content). This may be attributed to the high nonuniformity ($D_{90}/D_{10} = 6$) of the sediment mixture E60, leading to a more densely packed bed, as mentioned by Y. P. Chen et al. (2021). At velocity level 7, migrations of the ripple bed were observed, suggesting a bed load transport regime, indicative of an erosion behavior similar to sandy beds. The ripples were mainly composed of coarse sediment grains (e.g., $D_{50} = 97$ μm for sediment mixture E29) with dark colors compared to the original bed mixtures, indicating near-bed sorting processes. The fine grains were transported upward as a suspended load, leaving the coarse grains at the bed surface and forming ripples. This is slightly different from the segregation of grain sizes in graded sandy bed mixtures as shown in May et al. (2010) and Thomas (2000). In graded sandy bed mixtures, sandy grains are mainly transported as bed loads, and the fine grains can percolate through pores between coarse grains during transportation, eventually forming a coarse surface layer.

3.2. Development of the *SSC*

The vertical distribution of the *SSC* in the annular flume is nearly uniform, which is different from the long-straight flume. Herein, developments of the *SSC* at different velocity levels are represented by the measurement at the level of ~ 2.95 cmab. Figure 3 illustrates temporal changes in the *SSC* at different velocity levels, taking sediment

mixtures E29, E49, and E66 as examples. Data were masked out during flow adjustment when altering the rotation speed of the flume.

For sediment mixture E29 (29% silt content, Figure 3c), when the flow velocity is low (i.e., velocity levels 1–3), the *SSC*s were extremely low and exhibited certain fluctuation characteristics. This is because the ambient water contains a very small amount of substances in the water, which can be captured by the optical sensors. These *SSC*s are recognized as the background concentration. At velocity levels 4–7, the *SSC*s become recognizable and gradually increase to a stable level at each certain velocity level. The stable *SSC*s correspondingly increase with velocity, but the development of a stable *SSC* requires more time for a larger velocity. In particular, there is a sharp increase in *SSC* at velocity level 7 (Figure 3). This sharp increase in *SSC* is accompanied by the occurrence of ripples, as shown in Figure 2. Ripples can enhance near-bed turbulence by introducing more sediment suspended from the bed.

When the silt content increases in the bed (i.e., 49% in Figure 3b and 66% in Figure 3a), the increasing trend of the *SSC* with increasing flow velocity is similar to that of sediment mixture E29, but there is a delay tendency for *SSC*
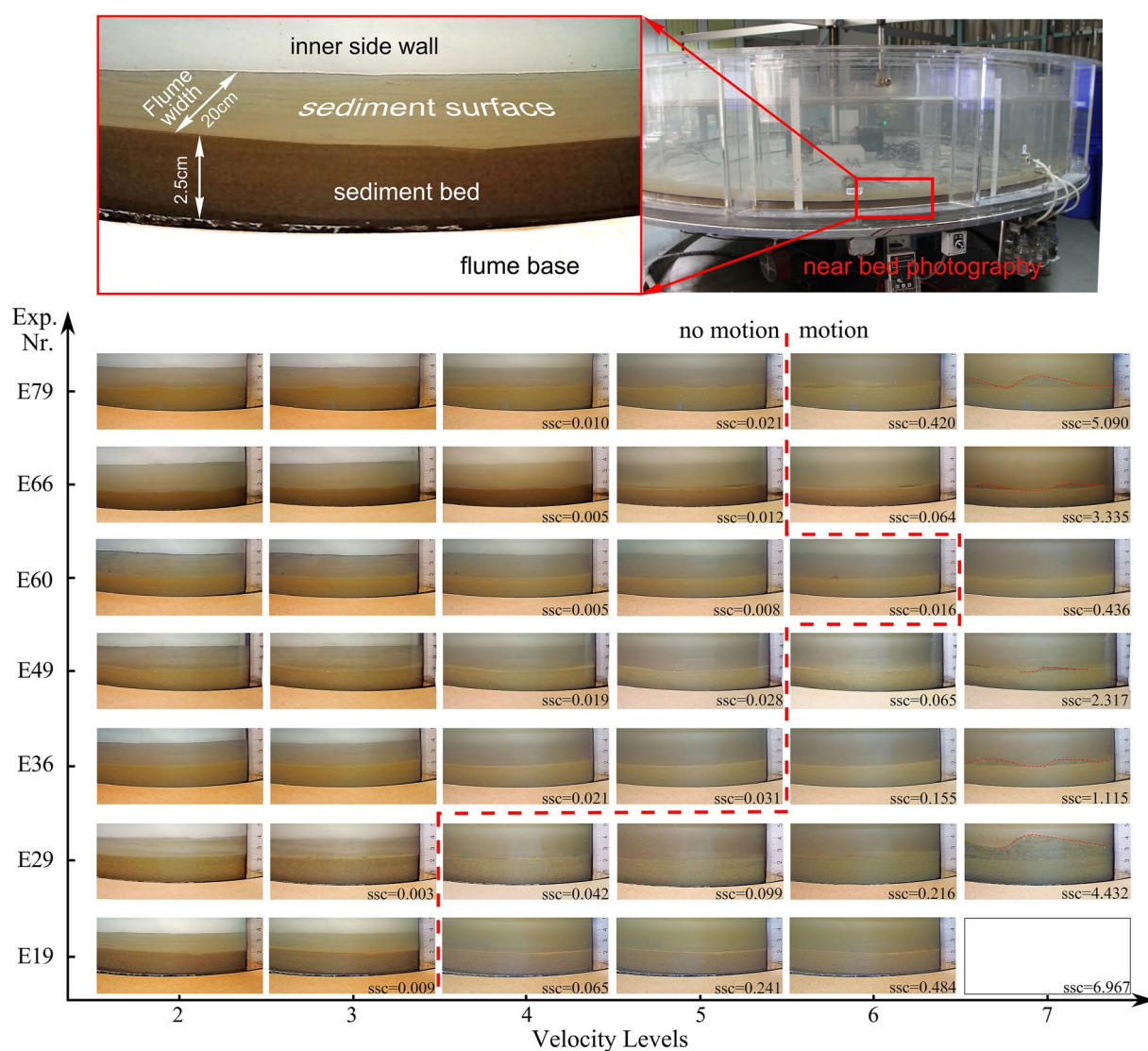
Figure 2. Close-up photos near the sediment bed taken during steady state at each velocity level over different sand-silt mixtures. The upper panel denotes where these photos were taken. In the lower panel, the red dashed line is a dividing line denoting motion and no motion. The suspended sediment concentrations (*SSC*s) labeled in each subfigure was measured by infrared backscatter sensors (*IBS*s) with units of kg/m³. The camera ran out of power at velocity level 7 over sediment bed E19 (19% silt). Note that there may be variations in the brightness of the photos in different groups of experiments.
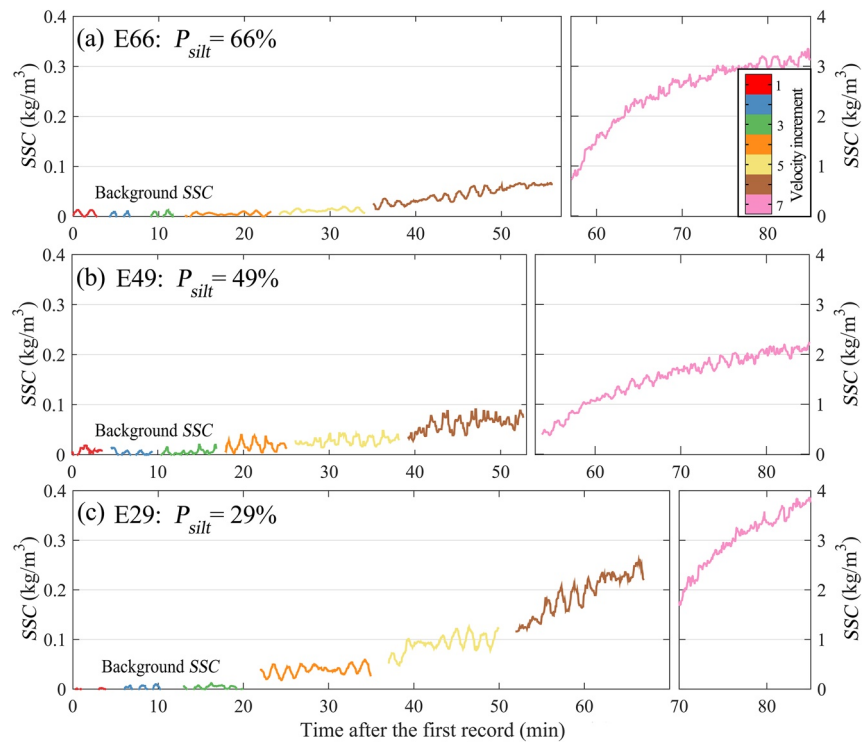
Figure 3. Development of suspended sediment concentrations (*SSC*s) at each velocity level over sediment mixtures E29, E49, and E66. Colors represent different velocity levels.

increase. For example, the *SSC* is approximately 0.05 kg/m³ at velocity level 4 over sediment mixture E29 (29% silt content), whereas the same magnitude of *SSC* can only be achieved at velocity level 6 for sediment mixtures E49 and E66 (with 49% and 66% silt content, respectively). At velocity level 7, there is also a sharp increase in *SSC* for sediment mixtures E49 and E66, but the cost time for developing to the equilibrium state varies.

3.3. Development of Bed Morphology

Figure 4 presents temporal changes in the bed surface elevation at different velocity levels, taking sediment mixtures E29, E49, and E66 as examples. In general, recognizable ripples were depicted at velocity level 7 for all these sediments. However, changes in bed morphology were found to be different for different sediment mixtures. For sediment mixture E29 (29% silt content), the bed surface was kept flat at velocity levels 1–5, but the surface elevation was reduced slightly since velocity level 3, indicating the initiation of erosion. Small-scale ripples, which cannot be visually observed in Figure 2, were detected by the *ADV* at velocity level 6. For sediment mixture E49 (49% silt content), there were slight fluctuations on the bed surface at velocity levels 4–6, but the reduction in the surface elevation was very small. For sediment E66 (66% silt content), the variations in the bed surface were similar to those of sediment E49 at velocity levels 4 and 5. However, very small-scale ripples were recognized at velocity level 6. These results indicate that when the silt content is increased from 35% to 50%, the bed becomes stable, whereas the mobility of the bed appears to be relatively increased when the silt content further increases from 50% to 70%.

3.4. Near Bed Hydrodynamics

Figure 5 presents velocity profiles at velocity levels 4 to 6 (when the sediment started to be eroded, as shown in Figure 2) over different sediment beds. In general, the velocity profiles exhibited more or less similar shapes. The velocity was reduced rapidly near the bed, showing a near-bed boundary layer effect. Meanwhile, under the same velocity level, the near-bed velocities were different over different sediment beds. To give a representative value of flow velocity at different levels, we averaged all depth-averaged velocities of each experiment and presented
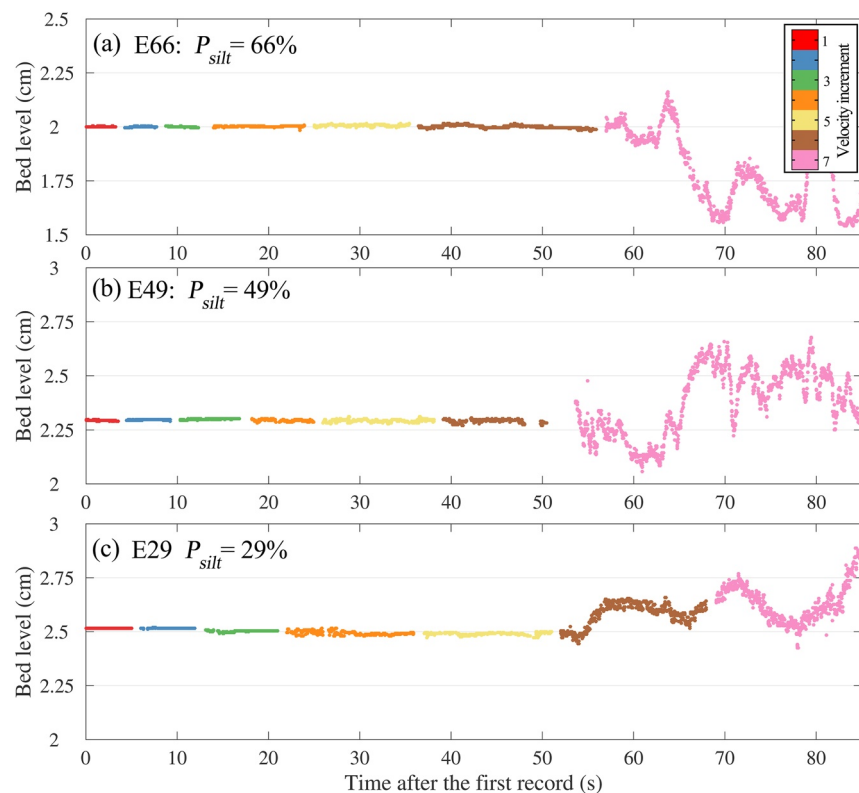
Figure 4. Variations in bed level at each velocity level over sediment mixtures E29, E49, and E66. The colors represent different velocity levels.

them in Figure 5. At velocity level 4 ($\overline{U}$ = 0.20 m/s), the lower part of the velocity profile of sediment mixture E19 (19% silt) was smaller than those in the other experiments, and the velocity gradient was larger. This indicates the onset of sediment bed changes (i.e., erosion starts) because part of the energy was consumed to maintain bed erosion. At velocity level 5 ($\overline{U}$ = 0.24 m/s), velocities over sediment mixtures E29 and E79 (29% and 79% of silt) were changed near the bed. At velocity level 6 ($\overline{U}$ = 0.27 m/s), sediment mixtures E19, E29, and E79 (19%, 29%, and 79% of silt content) were explicitly distinguished from other beds with reduced velocity magnitude. The *SSC*s in these three cases were 0.2–0.48 kg/m³ and small-scale ripples started to form. Thus, both *SSC* and bed roughness (composed of both grain and ripple-related roughness) influenced near-bed velocities. Furthermore, at velocity levels 4 to 6, velocities over sediment mixtures E36 to E66 appeared to be relatively stable and showed similar patterns. The *TKE* profiles near-bed were consistent with that of the open channel flow. That is, from the bed surface upwards, the *TKE* first increases and then gradually decreases, suggesting also a boundary layer effect. Comparison of both velocity and *TKE* profiles among different bed forms is important for future work to improve understanding on sediment dynamics near-bed, but this topic is beyond the scope of this study.

3.5. Critical Bed Shear Stress

As mentioned before, at each velocity level, the time series of the *SSC*s were measured at several locations along the flume. When the *SSC*s at each location became stable, we considered that the steady (equilibrium) state was achieved, and then the *SSC*s over a certain time (at least 5 min) were averaged. Meanwhile, the velocities were measured by the *ADV* profiler at a fixed location to calculate the bed shear stress. Figure 5 illustrates the relationship between the time-averaged *SSC* (taking the elevation of ~2.95 cmab as a reference) and the bed shear stress for different sediment mixtures. Generally, the *SSC* maintains a low value until a certain bed shear stress is achieved. The bed shear stress, at which *SSC* starts to increase, varies for different sediment beds. For example, *SSC* in experiments with mixtures E19 and E29 (19% and 29% silt content) began to increase at lower bed shear stress than in other experiments.
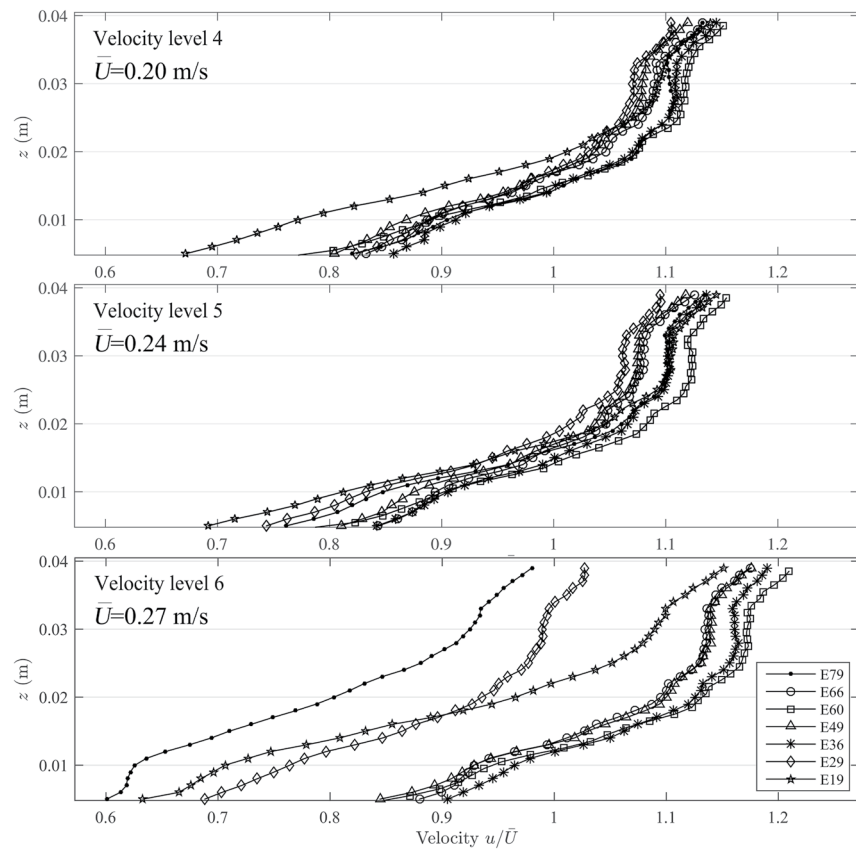
**Figure 5.** Near-bed velocity profiles over different sand-silt mixtures at velocity levels 4 to 6. z is the elevation above the sediment bed on a linear scale (log-scale refers to Figure S5 in Supporting Information S1).

As mentioned before, the critical *SSC* of 0.04 kg/m³ is used to identify the erosion threshold according to Figure 6. The derived critical bed shear stress is shown in Figure 7a. There is a sharp increase in critical bed shear stress at silt contents between 29% and 36%, whereas the critical bed shear stress exhibits fewer fluctuations with a further increase in silt content. The derived critical bed shear stresses of sediment mixtures E19 and E29 are more or less consistent with the Shields criterion (Figure 7b), whereas the critical bed shear stresses of other beds (silt content >35%) are much larger than the Shields value. Thus, the Shields criterion may not be applied to describe the erosion threshold for sand-silt mixtures with large silt contents. The error bars in Figure 7a denote standard
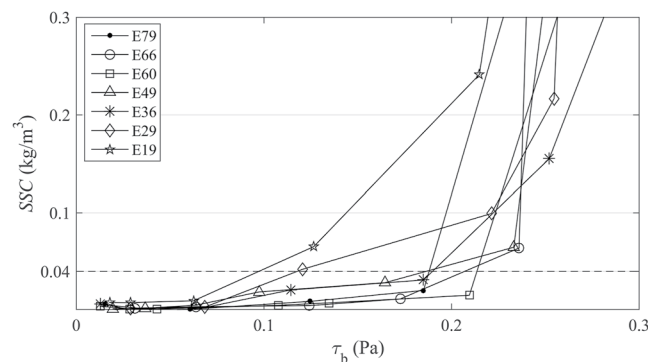
Figure 6. Relationship between time-averaged suspended sediment concentrations (*SSC*s) and bed shear stresses for different sediment mixtures. The dashed line denotes a critical *SSC* value of 0.04 kg/m³ for the determination of the critical bed shear stress.
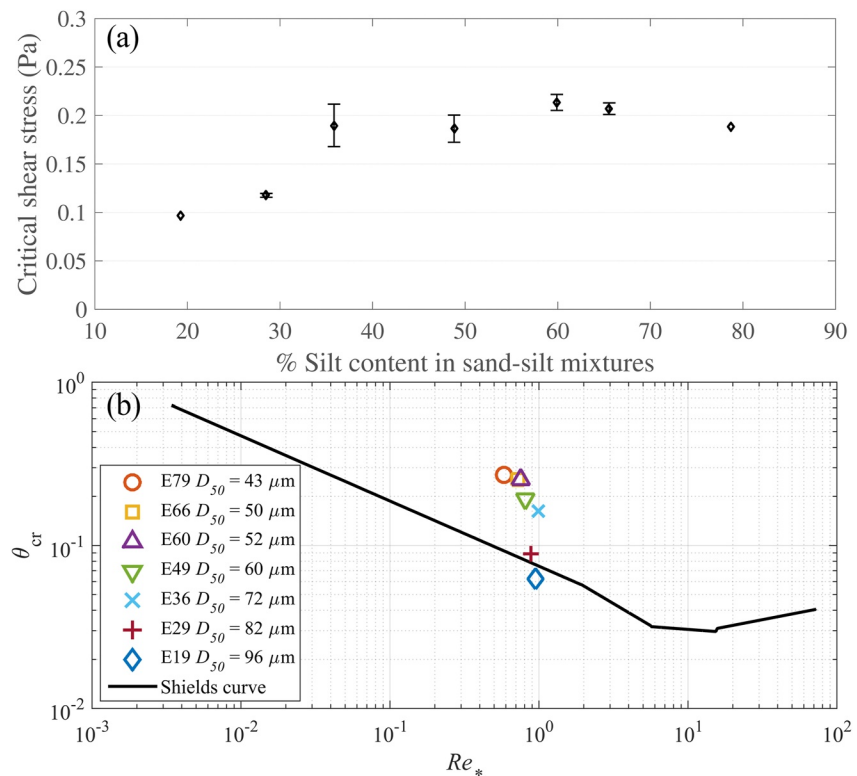
Figure 7. (a) Critical bed shear stress of sand-silt mixtures with different silt contents and (b) comparison with the Shields curve. The error bars in (a) are standard deviations based on repeated experiments. For sediment mixtures E19 and E79, no error analysis was performed because only two replicates were carried out in these two groups. Note that the data in (b) are the mean value of repeated experiments, and the solid line is based on the parametric method for the Shields curve proposed by van Rijn (2007a); see the Appendix A for details.

deviations based on repeated experiments. Since both the flume rotation speed and data processing are the same for each group, the errors should be attributed to small differences in initial bed composition in repeated experiments. Notably, the data point of E36 (~36% silt) has a relatively larger error bar than the others. On the one hand, this indicates that the small fluctuation in silt content can cause a relatively large experimental uncertainty. On the other hand, this further implies that a silt content of ~36% may serve as a tipping point; that is, a slight shift results in a large change in the critical bed shear stress.

3.6. Bed Properties

Bed properties, such as dry bulk density and permeability, are considered to play roles in the erosion behavior of fine sediment beds (Winterwerp & van Kesteren, 2004). In this study, dry bulk density, permeability, and scanning electron microscopy (*SEM*) images of sediment samples were measured and analyzed. Figure 8 shows the changes in dry bulk density and permeability with silt content. A significant drop in dry bulk density appears when the silt content is larger than 35% (Figure 8a). When the silt content is between 40% and 80%, the dry bulk density of the bed is similar (~1,400 kg/m^3), whereas when the silt content is smaller than 35%, the dry bulk density of the bed is similar as well (~1,650 kg/m^3). As mentioned before, the sand-silt mixture deposits rapidly approach the maximum compacting state by comparing the dry bulk density after 1 hr with its maximum value. Since the silty bed compacts rapidly, permeability was only measured at a dry bulk density of ~1,500 kg/m^3. Similar to the dry bulk density, the permeability first decreased and then remained constant with increasing silt content (Figure 8b). Overall, the permeabilities of the sand-silt mixtures were approximately $2.17 \times 10^{-6} \sim 4.90 \times 10^{-6}$ m/s, which are an order of magnitude larger than those of the clay-dominated bed.

SEM images were taken for each sediment sample to investigate the microstructure of the sediment bed with different silt contents (Figure 9). The *SEM* images illustrate that there are mainly two types of shapes of single
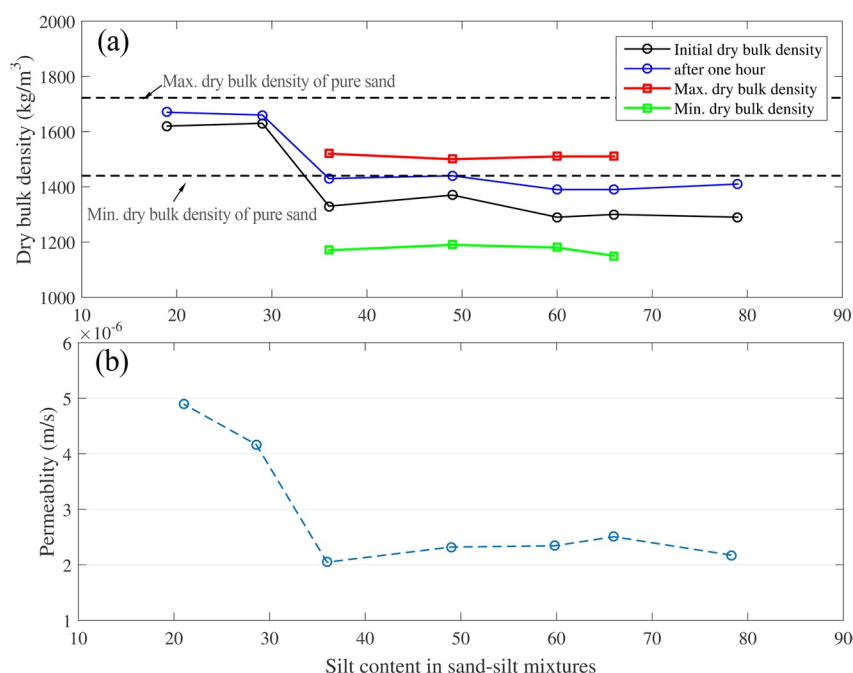
Figure 8. (a) Dry bulk densities and (b) permeabilities of different sand-silt mixtures. The permeabilities of sediment mixtures E36-E66 were measured at a constant dry bulk density of ~1,500 kg/m^3.

silt grains, namely, round shapes with rough surfaces and flat shapes with smooth surfaces and sharp edges. The packing structure of sand-silt mixtures is mainly the stacking arrangement between particles of different shapes and sizes. Furthermore, there are neither clay coating structures nor bio-organic matter (i.e., biofilm coated, see X. D. Chen et al., 2017; Fang et al., 2017) on the *SEM* images. As mentioned before, particles in the mixture smaller than 8 μm have been substantially removed artificially to exclude the effect of clay materials. These *SEM* images demonstrate that the cohesive materials in the mixture are extremely limited.

4. Discussion

4.1. Determination of the Erosion Threshold

The critical bed shear stress (τ_{cr}) has been commonly used to represent the erosion threshold. For sandy grains, the erosion threshold may be visually judged and then converted to the standard Shields criterion, while for fine-grained sediment, visual detection is rather difficult because the fine grains can be suspended directly when initiated and the water becomes turbid. Hence, the erosion threshold of fine-grained sediment has been widely estimated by extrapolating relations between bed shear stress and *SSC* or relations between bed shear stress and erosion rate by defining either a critical erosion rate (e.g., Mohr et al., 2018; Roberts et al., 1998) or a critical *SSC* (e.g., Amos et al., 1997; Staudt et al., 2017). However, definitions of either critical erosion rate or critical *SSC* vary significantly in different studies. For example, the critical erosion rate was ~10^{-4} cm/s in Roberts
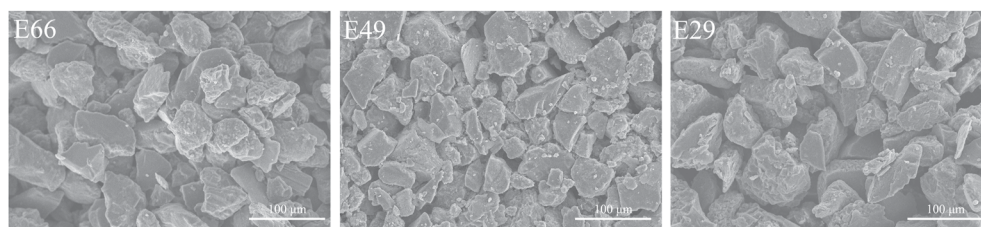
Figure 9. Scanning electron microscopy (*SEM*) images of sediment mixtures E29, E49, and E66.

et al. (1998) and ~10^{-5} cm/s in Mohr et al. (2018). The differences may be attributed to the bed materials and the judgment of the initiation of erosion.

Since the critical *SSC* is important for the accuracy of the resulting τ_{cr}, it is necessary to ensure its rationality. In this study, we defined the erosion threshold of sand-silt mixtures by relating the bed shear stress-*SSC* curve to the standard definition of the Shields criterion. The critical bed shear stress for the sand-dominated mixture E19 ($D_{50} = 96$ μm, silt content of 19%) estimated by the critical *SSC* of 0.04 kg/m³ was in good agreement with the Shields criterion (Figure 7b). The rationality of the critical *SSC* value for sediment mixture E19 has been further confirmed by the sudden increase in the *SSC* at velocity level 4 (Figure 2) and the reduction in near-bed velocity (Figure 5). This critical *SSC* is therefore used as a unified criterion for each type of sediment to guarantee comparability of the data between the experimental groups. As shown in Figure 2, for most sediment beds, the initiation of erosion occurred at velocity level 6, during which there was a sudden increase in the *SSC* and onset of fluctuations at the bed level (e.g., see sediment mixtures E49 and E66 in Figures 3 and 4, respectively). During velocity level 7, the *SSC* increased significantly for all sediment beds with the development of rippled beds. This indicates that for velocity level 7, all types of sediment mixtures were initiated into motion in the transport regime of both suspended and bed loads. Therefore, in this study, the determination of the erosion threshold is reliable by comparisons of time-series SSCs and bed level changes, close-up video recordings and near-bed velocity profiles. Furthermore, each group of experiments was repeated several times, and the error bars in Figure 7a also confirm the repeatability of the detection of the erosion threshold.

4.2. Erosion Threshold of Sand-Silt Mixtures

4.2.1. Importance of the Silt Content on the Erosion Threshold of Sand-Silt Mixtures

To further explore the erosion behavior of silt-sized sediment, existing data (Roberts et al., 1998; White, 1970) and data from the present study were analyzed. These data were recompiled and plotted against our experiments on both the Shields curve (Figure 10a) and the D_{50}-τ_{cr} curve. The sediments of these experiments have a unimodal shape with regard to the grain size distribution, which is common in coastal regions (Figure S1 in Supporting Information S1). The difference is that, in the present study, we aim to understand the effects of sediment composition, represented by different silt contents. Meanwhile, particles smaller than 8 μm were washed out before testing to exclude the influence of the clay material.

The present study depicts an increase in the erosion threshold for a silt content increasing from 20% to 35% and a near constant value when the silt content is larger than approximately 35% (Figure 7a), which is not shown in the data of Roberts et al. (1998) and White (1970) (Figure 10). For sediment mixtures with a smaller silt content (<35%), the erosion threshold can be well estimated by the Shields criterion. However, the Shield criterion underestimates the erosion threshold when the silt content is larger than 35% (Figures 7b and 10a). Therefore,
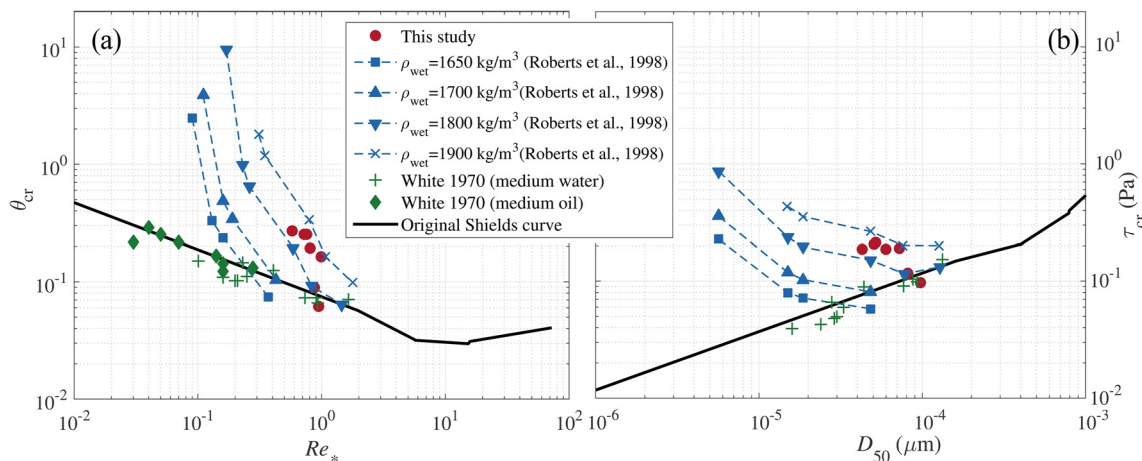
Figure 10. Comparison of existing data and data from this study in terms of (a) Shields curve and (b) critical bed shear stress over D_{50}.

the erosion behavior of sand-silt mixtures starts differing from that of noncohesive sand, exhibiting features of cohesive sediment when the silt content exceeds a threshold value (i.e., ~35% in this study).

From a geotechnical point of view, Karim and Alam (2017) found experimentally that an increase in the silt content reduces the undrained shear strength until a critical silt content of 30% and then the shear strength remains nearly unchanged until pure silt is reached. Jacobs et al. (2011) reported that the erosion threshold of sand-silt mixtures has a negative correlation with undrained shear strength. Thus, a decrease in undrained shear strength results in an increase in the erosion threshold.

4.2.2. Comparison With Existing Data

The study of White (1970) showed that the Shields curve fits fairly well with experimental data, even for fine silt (~16 μm), whereas the experiments of Roberts et al. (1998) and the present study suggest contradictory results on the erosion threshold, which is larger than the Shields criterion and increases with increased bulk density for silt-sized sediment (Figure 10). As mentioned by White (1970), the sediment bed was prepared by settling sediment grain by grain in weak flows (i.e., not causing erosion). That is, silty beds of White (1970) experiments may have a very low bulk density with loosely packed silt grains, which can be eroded individually. However, in the experiments of Roberts et al. (1998) and the present study, silty beds were allowed to settle for a certain period before the onset of flow. The Modern Yellow River Delta and the Jiangsu coast are two typical silt-dominated systems influenced by the silt-enriched Yellow River (Su et al., 2017a, 2017b). The silt content is approximately 48%–85% in the Modern Yellow River Delta (Jia et al., 2020) and 10%–80% along the Jiangsu coast (Kuai et al., 2021). Li and Cao (2009) reported that the wet bulk density of the deposit of a silty tidal flat (Rudong in the Jiangsu coast) is approximately 1.8 kg/m³ after 24 hr. This study further suggests that silt-sized sediment (at least for coarse silt, in this study, $D_{10} > 20$ μm) deposits rapidly and that the dry bulk density can be 90% of its maximum value after 1–2 hr (Figure S2 in Supporting Information S1 and Table 2), differing from a clay-dominated bed (i.e., compaction time scale of months). A deposition time of 1~2 hr, which corresponds to the duration of the slack water phase in a tidal-dominated environment, is sufficient for a silt-sized suspension to form a relatively stable bed. Thus, sand-silt mixtures in natural systems are rarely in a loosely packed state. Observations during this study showed that the sediment particles were eroded both collectively and individually. Hence, the bed configuration plays an important role in erosion threshold.

Comparison with Roberts et al. (1998) data (unimodal mixtures). In our experiments, dry bulk densities were 1,390–1,440 kg/m³ for mixtures with a silt content larger than 35% (i.e., sediment mixtures E36-E79). The resulting erosion threshold is consistent with Roberts' data in the case of a larger bulk density. Note that the data of Roberts et al. (1998) are based on wet bulk density (1,650–1,900 kg/m³), which is equivalent to a dry bulk density of 1,044–1,445 kg/m³. Furthermore, sediments in the experiments of Roberts et al. (1998) included fine silts ($D_{50} < 20$ μm, and percentage of clay-sized sediment >40%), of which the erosion threshold is strengthened significantly by larger bulk densities, indicating a behavior of clay-dominated sediments (Figure 10b). In our experiments, grains with sizes smaller than 8 μm were no more than 5%, resulting in a relatively small variation in bulk densities compared with the fine silts of Roberts et al. (1998). This implies that the erosion threshold of silt-sized sediment is located in a transition between cohesive and noncohesive sediment and depends on the compositions of the silty bed. For silts smaller than 20 μm, the deposition time scale would be longer than that of their coarse counterparts, and further study is required to understand the relevant influence on the erosion threshold.

Staudt et al. (2019) investigated the erosion behavior of various bimodal mixtures. One of their erosion experiments was performed with sediment mixtures composed of 40% silts ($D_{50} = 53$ μm) and 60% coarse sands ($D_{50} = 410$ μm). The sediment mixture exhibits a stabilized feature compared with the pure sandy bed. However, the *SSC*s began to increase (toward ~0.01 kg/m³) at the early velocity level with a bed shear stress of 0.014 Pa, but the bed remains flat for all velocity levels. This phenomenon indicates a selective transport of sand and silt for bimodal sediment mixtures; that is, silt is eroded separately through the pores of sandy grains. If a critical *SSC* of 0.04 kg/m³ is used to define the erosion threshold, then τ_{cr} of silt ($D_{50} = 53$ μm) is ~0.07 Pa, which is close to the Shields criterion (Figure 10). Thus, the silt fraction of bimodal sand-silt mixtures behaves as noncohesive sediment. The *RD* in Staudt et al. (2019) is 7.7, while that of this study is 2. This implies that the erosion of silts may vary with the grain size distribution of the sediment mixture. Understanding the erosion behavior of silts in both unimodal and bimodal sediment mixtures can be a future research topic.

4.3. Mechanisms Behind the Effects of Silt Content on the Erosion Threshold

It is widely accepted that network structure and cohesion are two influencing factors controlling the erosion behaviors of sand-clay mixtures (van Ledden et al., 2004). That is, cohesion introduced by clay materials would increase the erosion threshold of sand-clay mixtures, whereas an increase in clay can lead to a loosely packed bed (regarding fresh depositions) that reduces the erosion threshold. Regarding noncohesive bimodal sandy mixtures, geometrical interactions between fine and coarse grains can result in a stabilized network structure that enhances the erosion threshold, depending on the content of fines (Bartzke & Huhn, 2015). Bartzke and Huhn (2015) suggest that for bimodal sediment mixtures, when the content of fines is ∼30% by weight (in their case, D_{50} of coarse fraction = 600 μm and D_{50} of fine fraction = 80 μm), pore spaces between coarse grains can be completely filled, resulting in a maximum porewater flow blockage effects to stabilize the bed. However, when the pore spaces between coarse sand grains are not fully filled, the fine sediment can be transported at both the bed surface and inside the coarse-sand matrix. Thus, the enhancement for bed stabilization is weak.

Different from the existing study, the present study mainly focuses on the erosion behavior of unimodal sand-silt mixtures (i.e., $RD = 2$), and clay-sized fractions have been removed (<5%). Regarding network structures, because of the low grain-size ratio, the network structure of silt filling the pores of sand grains would not exist, as proven by the *SEM* images (Figure 9), which is different from the bimodal sand mixtures. Our experimental results indicated that the dry bulk density and permeability (representing the network structure of the bed mixtures) remain constant when the silt content is less than 35%, whereas they are reduced to another constant values when the silt content is greater than 35%. The variation in dry bulk density and permeability with silt content shows a similar trend as the erosion threshold of the sediment mixture, suggesting a strong correlation between them. Although the dry bulk density of the silty bed in this study is smaller than that of a sandy bed, the permeability is also reduced with increasing silt, which can slow down porewater flow and enhance bed stability. This is similar to the stabilization mechanism of bimodal sand mixtures. According to Chapuis (2012), the permeability of nonplastic mixtures is controlled mainly by the effective diameter (D_{10}) and void ratio. Since sand-silt mixtures compacted rapidly (on the scale of hours), a stable void ratio was attained. Therefore, the enhancement of the erosion threshold may be largely due to the decreased permeability controlled by D_{10} or the grain size distribution.

Cohesion of the bed, to a large extent, depends on clay minerals, of which small size and flat shape result in large specific area and an electrical charge distribution (Winterwerp & van Kesteren, 2004). The cohesive force between clay particles can be described by diffusive double layer theory, which is a balance between intermolecular van der Waals attractive forces and repulsive electrical forces (due to negative charges on the particle's surface). In this study, particles smaller than 8 μm were very limited in the sand-silt mixtures, so the effects of clayey cohesion can be neglected. This can be further confirmed by settling experiments, which showed no obvious flocculation in freshwater. The SEM images also indicated that neither clay-dominated nor biological structures exist in the sand-silt mixtures (Figure 9). Therefore, clay minerals (i.e., electrochemical interaction) and biological matter-induced cohesive force is not responsible for the increased erosion threshold for the silt-dominated bed.

From a mechanical point of view, Jang and Santamarina (2016) summarized that silt as small as 20 μm has low plasticity and low electrical sensitivity. That is, the electrochemical force controlling clayey grains may be weak for silt, at least for silt with sizes larger than 20 μm. On the other hand, Dou (1960) proved the existence of attractive forces between coarse silty grains (∼60 μm) by experiments of cross-quartz wires. Hence, there is still a certain attraction (i.e., van der Waals forces) between the two closely adjacent silt-sized particles, which is comparable to gravity force. Since silt has a smaller size but compacts rapidly (closely packed state), silt-sized grains are expected to form a stable silt skeleton (SS) that can resist erosion. This study suggests that the silt skeleton becomes more effective when the silt content is larger than 35% in the mixed bed, leading to an enhanced erosion threshold. Meanwhile, when the silt content is smaller (i.e., sediment mixtures E19-E29), the attraction force would be too weak to form such a silt skeleton to resist erosion. Therefore, the corresponding erosion threshold is consistent with the Shields curve.

4.4. Prediction of the Erosion Threshold for Silt-Dominated Mixtures

For practical modeling purposes, critical bed shear stress (τ_{cr}) is an important parameter for the prediction of sediment transport, bridging the gap between laboratory experiments and field surveys. To examine whether

existing formulas can predict critical bed shear stress for sand-silt mixtures with unimodal grain size distribution, several widely used formulas for mixtures have been chosen, that is, Soulsby and Whitehouse (1997, referred to as SW97), Van Rijn (2007a, referred to as VR07), Dou (2000, referred to as Dou00) and Wu et al. (2018, referred to as Wu18). The SW97 formula adopted a direct curve fitting method between the Shields parameter and particle sizes. The other three formulas basically treat the mud fraction (i.e., <62.5 μm) as cohesive and consider the mud effects on the original Shields curve for sand in the following form (as summarized by Wu et al., 2018):

$$\tau_{cr} = \lambda_1 \tau_{cr,o} + \lambda_2 \tau_{cr,mud} \text{ or } \tau_{cr} = (1 + \lambda_3)\, \tau_{cr,o} \tag{2}$$

where τ_{cr} is the critical bed shear stress of the mixtures; $\tau_{cr,o}$ is the critical bed shear stress calculated by the Shields curve, based on D_{50} of the mixed bed for unimodal mixtures or D_{50} of the sand fraction for bimodal mixtures; $\tau_{cr,mud}$ is the critical bed shear stress of the mud fraction; λ_1, λ_2 and λ_3 are parameters that relate to mud content and can be calculated by different functions in different formulas. The detailed information on these formulas is listed in the Appendix A.

Figure 11 presents the results of these formulas on critical bed shear stress for the sand-silt mixtures. All of the computed critical bed shear stresses show an increasing trend with decreasing sediment size. SW97 and VR07 give underestimated results, whereas Dou00 provides overestimations. For sediment mixtures with silt contents lower than 35%, SW97 and VR07 as well as the Shield criterion could provide comparable results with experiments implying features of sand-dominated behavior. However, the sudden change in τ_{cr} when the silt content is larger than 35% is not captured by these formulas, suggesting a unique feature of silt-dominated mixtures. Although Wu18 generally produces overestimated results compared to measured data, the abrupt change when the silt content is approximately 35% is captured. This further demonstrates that the cohesiveness and network structure of silt-dominated mixtures are different from those of clay-dominated mixtures, leading to different erosion behaviors. It is worth noting that all these aforementioned formulas are calibrated by erosion experiments over clay-dominated mixtures. This is the major reason for the deviation between the existing formulas and the experimental data of sand-silt mixtures.

To account for the unique erosion behavior of silt-dominated mixtures, a modified Shields criterion is deduced as follows. As discussed in the previous section, van der Waal forces can be comparable to gravitational forces for silt-sized sediment and should be considered. The van der Waal force between two spherical particles can be written as (Israelachvili, 2011):

$$F_c = \frac{A_h D_{50}}{24 r^2} \tag{3}$$

where A_h is the Hamaker constant and r is the distance between the two spheres. A_h depends on the materials and pore filling medium (e.g., water or air). For example, the A_h value for crystalline quartz (silt mineral) in water is ~1.7 × 10⁻²⁰ J but is ~3.1 × 10⁻²⁰ J for kaolinite (clay mineral; Miedema, 2013). Sediment beds are usually composed of different minerals with different shapes, sizes, etc., so it is difficult to obtain a constant A_h. Dou (2000) proposed a similar formula to account for cohesive forces:

$$F_c = \alpha_c \rho_w D_{50} \varepsilon \left(\frac{\rho_{dry}}{\rho_{stable}} \right)^\beta \tag{4}$$
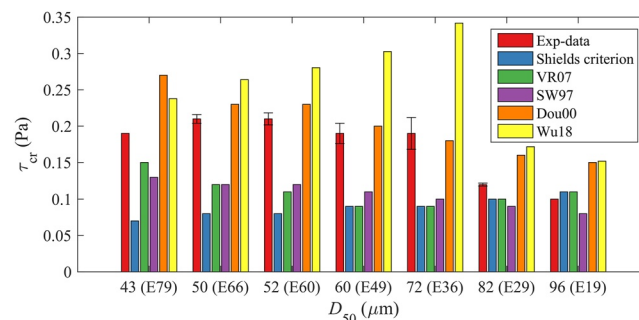
Figure 11. Comparison of computed critical bed shear stress by existing formulas with experimental data for the sand-silt mixtures.

where ρ_w is the water density; ρ_{dry} is the dry bulk density; ρ_{stable} is the stable dry bulk density, which refers to the maximum density for the fully consolidated bed for cohesive sediment; ε is a cohesion parameter depending on materials (unit of m^3/s^2); α_c and β are coefficients that are different in different studies. For sand-silt mixtures with limited clay materials, this study shows a rapid deposition process to a stable state. Thus, $\frac{\rho_{dry}}{\rho_{stable}} \approx 1$ in this case, and Equation 4 can be rewritten as:

$$F_c = \alpha_c \rho_w D_{50} \varepsilon \tag{5}$$

Equation 5 can be further interpreted as the aforementioned silt-skeleton force enhancing the erosion threshold of mixtures with silt contents larger than 35%. Subsequently, a modified Shields parameter can be derived by adding Equation 5 to the force balance equation of sediment particles:

$$\frac{\tau_{cr}}{(\rho_s - \rho_w)\, g\, D_{50} + \alpha \frac{\rho_w}{D_{50}}} = f\,(\mathrm{Re}_*) \tag{6}$$

where ρ_s is the sediment density; g is the gravity acceleration; the left-hand side of Equation 6 refers to the modified Shields parameter (i.e., θ_{cr}), and the right-hand side is the function of the grain Reynolds number (Re$_*$), which can be calculated according to the dimensionless diameter D_* (van Rijn, 2007a, see Equation A3). $\alpha = k_1 \varepsilon$ (unit of m^3/s^2) can be considered an expanded cohesive parameter, and its value varies for different materials. Since the cohesion parameter ε depends on material properties (e.g., the minerology, sphericity, surface roughness, and orientation of grains) and is difficult to determine theoretically, existing data sets, such as those from Dou (2000), Jia et al. (2020), and Roberts et al. (1998) and the present study, were used to determine α for the sand-silt mixtures. Curve fitting depicts $\alpha = 5.2 \times 10^{-8}$ m^3/s^2 with an R^2 of 0.658 by setting the intercept to 0, while $\alpha = 3.8 \times 10^{-8}$ m^3/s^2 ($R^2 = 0.822$) has a fitted intercept of 0.43. Fitting curves refer to Figures S6 and S7 in in Supporting Information S1. The physical meaning of the intercept can be interpreted as an enhancement of gravity force due to reduced permeability (i.e., reduced pore water flow) with increased silt content. Nevertheless, the differences in whether to consider this item are within 10%, indicating that the intercept can be ignored for sand-silt mixtures. Note that this modified formula only applied for beds with silt content >35%. The Shields criterion can be adopted for mixtures with silt content <35%. Thus, the resulting critical bed shear stress can be written as:

$$\begin{cases} \tau_{cr} = \tau_{cr,o}, & \text{for silt content } < 35\% \text{ (sand-dominated)} \\ \tau_{cr} = (1 + \beta_{SS})\, \tau_{cr,o}, & \text{for silt content } \geq 35\% \text{ (silt-dominated)} \end{cases} \tag{7}$$

where τ_{cr} is the critical bed shear stress for sand-silt mixtures and $\tau_{cr,o}$ is the critical bed shear stress by the Shields criterion (see Van Rijn, 2007a). β_{SS} is a dimensionless parameter representing the effects of the silt-structural force, and $\beta_{SS} = \frac{\alpha}{(s-1)g D_{50}^2}$ with $\alpha = 5.2 \times 10^{-8}$ m^3/s^2. s is the relative density of sediment grains ($s = \rho_s/\rho_w$). It is noted that Equation 7 still follows the form of previous studies for the sand-mud mixtures shown in Equation 2.

The grain size distribution of bed materials in silt-dominated systems is unimodal, so the median grain size D_{50} is closely related to the grain size distribution. In some data-poor regions, it is common that D_{50} is the only parameter recording information of the bed material, making application of Equation 7 difficult. To this end, it is better to derive a relationship between D_{50} and the silt content in mixtures. We have collected and recompiled several field survey data on bed compositions in silt-dominated systems, such as the Jiangsu coast (Kuai et al., 2021) and Modern Yellow River Delta (Jia et al., 2020). Curve fitting between D_{50} and silt content in mixtures depicts a negative and linear relationship ($R^2 = 0.996$). The 35% silt content, beyond which the bed would be transitioned to silt-dominated, corresponds to a D_{50} of 73 µm, which is close to the 75 µm size discriminator of sand and silt in geotechnical engineering (Santamarina et al., 2001). Thus, the erosion threshold for unimodal sand-silt mixtures can be written as follows:

$$\begin{cases} \tau_{cr} = \tau_{cr,o}, & \text{for particles } \geq 75\,\mu\text{m (sand-dominated)} \\ \tau_{cr} = (1 + \beta_{SS})\, \tau_{cr,o}, & \text{for particles between 20 and 75}\,\mu\text{m (silt-dominated)} \end{cases} \tag{8}$$

Note that Figure 12 suggests that the minimum D_{50} is approximately 20 µm for typical silt-dominated systems. This implies that a further decrease in D_{50} would inevitably increase the content of fines smaller than 20 µm, which may change the mixture from silt-dominated to clay-dominated. Furthermore, since the relationship between the
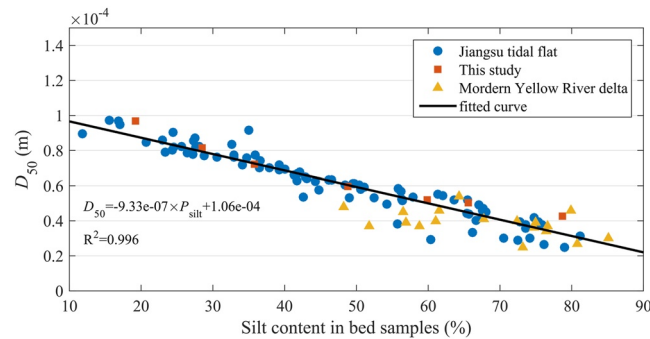
Figure 12. Relationship between the median grain size and silt content in bed samples of silt-dominated coasts.

silt content and D_{50} is fitted only by two data sets, Equation 8 should be used with care, but Equation 7 is in a more general manner. More data are required to validate Equation 8. Figure 13 shows the performance of the proposed formula (i.e., Equation 7 or Equation 8), which can fit the data well over unimodal sand-silt mixtures with sediment sizes between 20 and 100 μm. The percentage bias between the predictions and measured data is within 10%, which is better than that of VR07 (65%) and Dou00 (30%). The newly proposed formula produces an intermediate value between VR07 (i.e., Equation A2) and Dou00 (Equation A4), Furthermore, the proposed formula captures abrupt changes in the erosion threshold from sand-dominated to silt-dominated mixtures by a critical D_{50}. Since the data do not cover fine silts (<20 μm), whether the proposed formula can be extended to fine silts is unclear and requires further study.

Notably, the clay minerals in the sediment mixtures in this study are rather limited. In natural systems, sediment minerals, water salinities, biological effects, etc., may also contribute to the erosion behavior of sand-silt mixtures to a certain extent. For example, biofilm-coated sediment exhibits stronger cohesive features than clay minerals (Fang et al., 2017), while salinity may cause flocculation on fine-grained sediment, delaying bed compaction processes. The effect of these factors on the erosion threshold of sand-silt mixtures should be taken into account in the future but beyond the scope of this study.

5. Conclusions

A series of erosion experiments were carried out to explore the transitional erosion behavior of sand-silt mixtures. Different bed compositions were prepared with limited clay contents. The critical bed shear stress was adopted to represent the erosion threshold, which was detected collectively by the measured SSCs, near-bed velocities and bed levels over different velocity levels. These measured variables also suggest an increase in critical shear stress for erosion when the silt content of the bed is larger than 35%. This silt content was found to be a tipping point, beyond which the critical bed shear stress increased abruptly and then maintained a constant value until
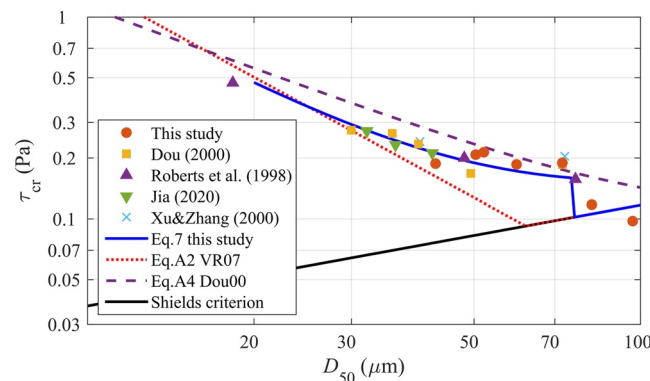
Figure 13. Comparison of the newly proposed formula (i.e., Equation 8) with experimental data of sand-silt mixtures and existing formulas.

a pure silty bed was reached. Furthermore, the bed network structure was changed from sand-dominated to silt-dominated beyond this silt content, as indicated by the dry bulk density and bed permeability.

By combining existing data with the present experimental data, we confirmed that the composition of silty beds is an important factor that controls the transitional erosion behavior of sand-silt mixtures. When the silt content exceeds the critical value, a stable silt skeleton is formed by the attraction force chain increasing the bed resistance for erosion, whereas the attraction force chain is too weak to be effective for the sand-dominated bed. Based on this assumption, a modified formula taking silt content into account has been deduced to estimate the critical bed shear stress. For natural silt-dominated systems, a bed with a silt content of 35% corresponds to a median grain size of 75 μm, which further favors practical applications.

The smallest grains inside the sand-silt mixtures used in this study are ∼20 μm (i.e., D_{10}). Thus, we concentrate on the erosion behavior of coarse silts, which are found to deposit rapidly (sand-like) but are difficult to erode (clay-like). In fine-grained muddy tidal flats, bed materials may also be enriched in fine silts, clay, and organic matter. On the one hand, the further increase in these fine grains would inevitably change the bed compositions and decrease the median grain size. On the other hand, how fine silts interact with coarse silts as well as with clays on erosion behavior requires further studies for a better understanding of mixed sediment transport.

Appendix A: Formulas for Prediction of Critical Bed Shear Stress

Soulsby and Whitehouse (1997) proposed a generalized formula extending Shields curve for very fine grains ($D_* < 1$):

$$\frac{\tau_{cr}}{\left[(\rho_s - \rho_w) g D_{50}\right]} = \frac{0.3}{1 + 1.2 D_*} + 0.055 \left[1 - \exp\left(-0.020 D_*\right)\right], \tag{A1}$$

where, D_{50} is the median diameter of sediment bed; $D_* = D_{50}\left[(s-1)g/\nu^2\right]^{1/3}$ is dimensionless particle size; ν is the kinematic viscosity coefficient.

Van Rijn (2007a) proposed the following formulas to calculated critical bed shear stress accounting influences of both network structure and cohesion for sediment smaller than 62 μm:

$$\tau_{cr} = \begin{cases} \left(c_{gel}/c_{gel,s}\right)\left(D_{sand}/D_{50}\right)^{\gamma} \tau_{cr,o}, & \text{for } D_{50} < 62 \, \mu m \\ \left(1 + P_{clay}\right)^3 \tau_{cr,o}, & \text{for } D_{50} \geq 62 \, \mu m \end{cases}, \tag{A2}$$

in which, c_{gel} is the gelling mass concentration of fine sediments (<62 μm), and $c_{gel} = (D_{50}/D_{sand}) c_{gel,s}$, with $c_{gel,min} = 120$ kg/m³; $c_{gel,s}$ is the dry bulk density of sand bed by mass (1,722 kg/m³); γ is a calibration factor and $\gamma = 2$ in this study. In this study, $c_{gel}/c_{gel,s} = 1$ because of rapid compaction process of sand-silt mixtures. $\tau_{cr,o}$ is the original critical bed shear stress based on a revised parametric Shields curve:

$$\frac{\tau_{cr,o}}{\left[(\rho_s - \rho_w) g D_{50,bed}\right]} = \begin{cases} 0.115 D_*^{-0.5}, & D_* \leq 4 \\ 0.14 D_*^{-0.64}, & 4 < D_* \leq 10 \\ 0.04 D_*^{-0.1}, & 10 < D_* \leq 20 \\ 0.013 D_*^{0.29}, & 20 < D_* \leq 150 \\ 0.055, & 150 < D_* \end{cases} \tag{A3}$$

Dou (2000) proposed a uniformed formula by introducing cohesive force and stable bulk density to calculated $\tau_{cr,bed}$ for both non-cohesive and cohesive sediments:

$$\tau_{cr} = p^2 \rho_w \left(\frac{\Delta}{\Delta_*}\right)^{1/3} \left[3.6 \frac{\rho_s - \rho_w}{\rho_w} g D_{50} + \left(\frac{\rho_{dry}}{\rho_{stable}}\right)^{2.5} \left(\frac{\alpha_0 + gh\delta\sqrt{\delta/D_{50}}}{D_{50}}\right)\right], \tag{A4}$$

in which, p is the coefficient representing different stages of initiation of motion, that is, impending motion, little motion or general motion and $p^2 = 0.0164$ referring to little motion; Δ is the roughness height and $\Delta = 5 \times 10^{-4}$ m for sediments smaller than 500 μm; $\Delta_* = 1 \times 10^{-2}$ m; ρ_{stable} is stable dry bulk density and in this study, $\left(\frac{\rho_{\text{dry}}}{\rho_{\text{stable}}} \right)^{2.5} = 1$ in this study due to rapid compaction feature of sand-silt mixtures; $\alpha_0 = k_2 \varepsilon$ is an expanded cohesive parameter relating to physical and chemical properties of the particle materials and $\alpha_0 = 1.75 \times 10^{-6}$ m³/s² based on Dou ([2000]); h is the water depth; δ is the parameter of the water film thickness and $\delta = 2.31 \times 10^{-7}$ m.

Wu et al. ([2018]) proposed an empirical formula of critical bed shear stress for sand-mud mixtures, which is a function of the critical bed shear stress of pure sand and mud, mud content and sand diameter:

$$\tau_{\text{cr}} = \tau_{\text{cr},L} + (\tau_{\text{cr,mud}} - \tau_{\text{cr},L}) \exp \left[-\alpha_1 \left(\frac{P_{\text{sand}}}{P_{\text{mud}}} \right)^{1.2} \right], \tag{A5}$$

in which, $\tau_{\text{cr},L}$ is the critical bed shear stress for mixture with low mud content and $\tau_{\text{cr},L} = \tau_{\text{cr},o} + 1.25 \left(\tau_{\text{cr,mud}} - \tau_{\text{cr},o} \right) \min \left(P_{\text{mud}}, 0.05 \right)$; $\tau_{\text{cr,mud}}$ is the critical bed shear stress for pure mud and in calculation we use the experimental results of E79 (i.e., 79% of silt) as the $\tau_{\text{cr,mud}}$; α_1 is the empirical coefficient and $\alpha_1 = 0.42 \exp \left(-3.38 D_{50,\text{sand}} \right)$.

Notations

A_{h}	Hamaker constant
C_1	Coefficient describes the ratio between τ_b and *TKE*
c_{gel}	Gelling mass concentration of fine sediments (<62 μm)
$c_{\text{gel,s}}$	Dry bulk density of sand bed by mass, $c_{\text{gel,s}} = 1{,}722$ kg/m³ for pure sand
D_{10}	The portion of particles with diameters smaller than this value is 10%
D_{50}	The portion of particles with diameters smaller and larger than this value are 50%, also known as median grain size
D_{90}	The portion of particles with diameters below this value is 90%
$D_{50,\text{sand}}$	The median grain size of sand fraction within mixtures
$D_{50,\text{silt}}$	The median grain size of silt fraction within mixtures
D_{sand}	Separation diameter between sand and silt fraction, $D_{sand} = 62$ μm
D_*	The dimensionless diameter
F_c	van der Waal force between two spherical particles
g	Gravity acceleration
h	Water depth
k	Permeability
p	coefficient representing different stages of initiation of motion
P_{clay}	Percentage of clay fraction (<8 μm)
P_{mud}	Percentage of mud fraction (<62.5 μm)
P_{sand}	Percentage of sand fraction (>62.5 μm)
P_{silt}	Percentage of silt fraction (8 ~ 62.5 μm)
r	The distance between the two spheres
RD	The ratio of coarse grains over fines, $RD = D_{50,\text{sand}}/D_{50,\text{silt}}$
Re_*	Grain Reynolds number
s	Relative density of sediment grains, $s = \rho_s/\rho_w$
u'_x	Velocity fluctuations along-channel direction
u'_y	Velocity fluctuations in cross-channel direction
u'_z	Velocity fluctuations in vertical direction
$\overline{U}$	Depth averaged velocity
α	Expanded cohesive parameter in this study
α_0	Expanded cohesive parameter in Dou ([2000]).
α_1	Coefficient in Equation [A5]
α_{c}	Coefficient for calculation of cohesive force

β	Empirical coefficient in Equation 4
β_{SS}	Dimensionless parameter representing the effects of Silt-Structural force
γ	Calibration factor in Equation A2
δ	Parameter of the water film thickness
Δ	Roughness height
Δ_*	Reference roughness height and $\Delta_* = 1 \times 10^{-2}$ m
ε	Cohesion parameter depending on materials
θ_{cr}	Critical Shields parameter
$\lambda_1, \lambda_2, \lambda_3$	Coefficients in Equation 2
ν	Kinematic viscosity coefficient
ρ_{dry}	Dry bulk density
ρ_s	Sediment density
ρ_{stable}	Stable dry bulk density
ρ_w	Water density
ρ_{wet}	Wet bulk density
τ_b	Bed shear stress
τ_{cr}	Critical bed shear stress
$\tau_{cr,L}$	Critical bed shear stress for mixture of low mud content
$\tau_{cr,mud}$	Critical bed shear stress of the mud fraction
$\tau_{cr,o}$	Critical bed shear stress calculated by the Shields curve
TKE	Turbulence kinetic energy
SSC	Suspended sediment concentration
LP	Log profile method
COV	Reynolds stress method
DDL	Diffusive Double Layer
SEM	Scanning Electron Microscope

Data Availability Statement

The experimental data sets for the sand-silt mixtures are available from the following link: https://doi.org/10.6084/m9.figshare.20285763.v1.

References

Amos, C. L., Feeney, T., Sutherland, T. F., & Luternauer, J. L. (1997). The stability of fine-grained sediments from the Fraser River Delta. *Estuarine, Coastal and Shelf Science*, *45*(4), 507–524. https://doi.org/10.1006/ecss.1996.0193

Baar, A. W., Boechat Albernaz, M., van Dijk, W. M., & Kleinhans, M. G. (2019). Critical dependence of morphodynamic models of fluvial and tidal systems on empirical downslope sediment transport. *Nature Communications*, *10*(1), 4903. https://doi.org/10.1038/s41467-019-12753-x

Bartzke, G., Bryan, K. R., Pilditch, C. A., & Huhn, K. (2013). On the stabilizing influence of silt on sand beds. *Journal of Sedimentary Research*, *83*(8), 691–703. https://doi.org/10.2110/jsr.2013.57

Bartzke, G., & Huhn, K. (2015). A conceptual model of pore-space blockage in mixed sediments using a new numerical approach, with implications for sediment bed stabilization. *Geo-Marine Letters*, *35*(3), 189–202. https://doi.org/10.1007/s00367-015-0399-1

Booij, R. (1994). *Measurements of the flow field in a rotating annular flume (No. 0169–6548)*. TU Delft. Retrieved from http://resolver.tudelft.nl/uuid:431193bc-8cfb-46ce-81fd-5034941b0769

Buscombe, D., & Conley, D. C. (2012). Effective shear stress of graded sediments. *Water Resources Research*, *48*(5), W05506. https://doi.org/10.1029/2010WR010341

Chapuis, R. P. (2012). Predicting the saturated hydraulic conductivity of soils: A review. *Bulletin of Engineering Geology and the Environment*, *71*(3), 401–434. https://doi.org/10.1007/s10064-012-0418-7

Chen, X. D., Zhang, C. K., Paterson, D. M., Thompson, C. E. L., Townend, I. H., Gong, Z., et al. (2017). Hindered erosion: The biological mediation of noncohesive sediment behavior. *Water Resources Research*, *53*(6), 4787–4801. https://doi.org/10.1002/2016WR020105

Chen, Y. P., Qiao, Z. X., Xu, C. Y., & Yao, P. (2021). Influences of sediment composition on scour of silt-sand mixture bed. *Journal of Sediment Research*, *46*(5), 1–8. (in Chinese with English Abstract).

Dou, G. (1960). The theory for incipient motion of sediments. *Shuili Xuebao*, *4*, 44–60. (in Chinese).

Dou, G. (2000). Incipient motion of sediment under currents. *China Ocean Engineering*, *14*(4), 391–406.

Fagherazzi, S., Kirwan, M. L., Mudd, S. M., Guntenspergen, G. R., Temmerman, S., D'Alpaos, A., et al. (2012). Numerical models of salt marsh evolution: Ecological, geomorphic, and climatic factors. *Reviews of Geophysics*, *50*(1). https://doi.org/10.1029/2011RG000359

Fang, H. W., Lai, H. J., Cheng, W., Huang, L., & He, G. J. (2017). Modeling sediment transport with an integrated view of the biofilm effects. *Water Resources Research*, *53*(9), 7536–7557. https://doi.org/10.1002/2017WR020628

Goring, D., & Nikora, V. (2002). Despiking acoustic Doppler velocimeter data. *Journal of Hydraulic Engineering*, *128*(1), 117–126. https://doi.org/10.1061/(ASCE)0733-9429(2002)128:1(117)

Greenwood, B., & Xu, Z. (2001). Size fractionation by suspension transport: A large scale flume experiment with shoaling waves. *Marine Geology*, *176*(1–4), 157–174. https://doi.org/10.1016/S0025-3227(01)00159-1

Israelachvili, J. N. (2011). *Intermolecular and surface forces*. Academic Press.

Jacobs, W., Le Hir, P., Van Kesteren, W., & Cann, P. (2011). Erosion threshold of sand-mud mixtures. *Continental Shelf Research*, *31*(10, Supplement), S14–S25. https://doi.org/10.1016/j.csr.2010.05.012

Jang, J., & Santamarina, J. C. (2016). Fines classification based on sensitivity to pore-fluid chemistry. *Journal of Geotechnical and Geoenvironmental Engineering*, *142*(4), 06015018. https://doi.org/10.1061/(ASCE)GT.1943-5606.0001420

Jia, Y., Liu, X., Zhang, S., Shan, H., & Zheng, J. (2020). *Wave-forced sediment erosion and resuspension in the Yellow River Delta*. Singapore: Springer.

Karim, M. E., & Alam, M. J. (2017). Effect of nonplastic silt content on undrained shear strength of sand-silt mixtures. *International Journal of Geo-Engineering*, *8*(1), 14. https://doi.org/10.1186/s40703-017-0051-1

Kim, S., Friedrichs, C., Maa, J., & Wright, L. (2000). Estimating bottom stress in tidal boundary layer from acoustic Doppler velocimeter data. *Journal of Hydraulic Engineering*, *126*(6), 399–406. https://doi.org/10.1061/(ASCE)0733-9429(2000)126:6(399)

Kleinhans, M., & van Rijn, L. (2002). Stochastic prediction of sediment transport in sand-gravel bed rivers. *Journal of Hydraulic Engineering*, *128*(4), 412–425. https://doi.org/10.1061/(ASCE)0733-9429(2002)128:4(412)

Kramer, H. (1935). Sand mixtures and sand movement in fluvial model. *Transactions of the American Society of Civil Engineers*, *100*(1), 798–838. https://doi.org/10.1061/taceat.0004653

Kuai, Y., Tao, J., Zhou, Z., Aarninkhof, S., & Wang, Z. B. (2021). Sediment characteristics and intertidal beach slopes along the Jiangsu Coast, China. *Journal of Marine Science and Engineering*, *9*(3), 347. https://doi.org/10.3390/jmse9030347

Lamb, M. P., & Parsons, J. D. (2005). High-density suspensions formed under waves. *Journal of Sedimentary Research*, *75*(3), 386–397. https://doi.org/10.2110/jsr.2005.030

Lick, W., & McNeil, J. (2001). Effects of sediment bulk properties on erosion rates. *Science of the Total Environment*, *266*(1), 41–48. https://doi.org/10.1016/S0048-9697(00)00747-6

May, L. B. H., Golick, L. A., Phillips, K. C., Shearer, M., & Daniels, K. E. (2010). Shear-driven size segregation of granular materials: Modeling and experiment. *Physical Review E*, *81*(5), 051301. https://doi.org/10.1103/PhysRevE.81.051301

Miedema, S. A. (2013). Constructing the Shields curve: Part C—Cohesion by silt, V006T10A023. https://doi.org/10.1115/OMAE2013-10524

Miller, M. C., McCave, I. N., & Komar, P. D. (1977). Threshold of sediment motion under unidirectional currents. *Sedimentology*, *24*(4), 507–527. https://doi.org/10.1111/j.1365-3091.1977.tb00136.x

Mohr, H., Draper, S., White, D. J., & Cheng, L. (2018). The influence of permeability on the erosion rate of fine-grained marine sediments. *Coastal Engineering*, *140*, 124–135. https://doi.org/10.1016/j.coastaleng.2018.04.013

Panagiotopoulos, I., Voulgaris, G., & Collins, M. B. (1997). The influence of clay on the threshold of movement of fine sandy beds. *Coastal Engineering*, *32*(1), 19–43. https://doi.org/10.1016/S0378-3839(97)00013-6

Pope, N. D., Widdows, J., & Brinsley, M. D. (2006). Estimation of bed shear stress using the turbulent kinetic energy approach—A comparison of annular flume and field data. *Continental Shelf Research*, *26*(8), 959–970. https://doi.org/10.1016/j.csr.2006.02.010

Roberts, J., Jepsen, R., Gotthard, D., & Lick, W. (1998). Effects of particle size and bulk density on erosion of quartz particles. *Journal of Hydraulic Engineering*, *124*(12), 1261–1267. https://doi.org/10.1061/(asce)0733-9429(1998)124:12(1261)(1998)124:12(1261)

Santamarina, J. C., Klein, A., & Fam, M. A. (2001). *Soils and waves* (Vol. 1). New York: John Wiley & Sons. https://doi.org/10.1007/BF02987719

Shields, A. (1936). *Application of similarity principles and turbulence research to bed-load movement*. CalTech Library.

Soulsby, R. L. (1997). *Dynamics of marine sands: A manual for practical applications*. Thomas Telford.

Soulsby, R. L., & Whitehouse, R. J. S. (1997). Threshold of sediment motion in coastal environments. In *Pacific Coasts and Ports '97: Proceedings of the 13th Australasian Coastal and Ocean Engineering Conference and the 6th Australasian Port and Harbour Conference* (Vol. 1, pp. 149–154). Christchurch: University of Canterbury.

Staudt, F., Mullarney, J. C., Pilditch, C. A., & Huhn, K. (2017). The role of grain-size ratio in the mobility of mixed granular beds. *Geomorphology*, *278*, 314–328. https://doi.org/10.1016/j.geomorph.2016.11.015

Staudt, F., Mullarney, J. C., Pilditch, C. A., & Huhn, K. (2019). Effects of grain-size distribution and shape on sediment bed stability, near-bed flow, and bed microstructure. *Earth Surface Processes and Landforms*, *44*(5), 1100–1116. https://doi.org/10.1002/esp.4559

Su, M., Yao, P., Wang, Z. B., Zhang, C. K., Chen, Y. P., & Stive, M. J. F. (2016). Conversion of electro-optical signals to sediment concentration in a silt-sand suspension environment. *Coastal Engineering*, *114*, 284–294. https://doi.org/10.1016/j.coastaleng.2016.04.014

Su, M., Yao, P., Wang, Z. B., Zhang, C. K., & Stive, M. J. F. (2017a). Exploratory morphodynamic hindcast of the evolution of the Abandoned Yellow River delta, 1578–1855 CE. *Marine Geology*, *383*, 99–119. https://doi.org/10.1016/j.margeo.2016.11.007

Su, M., Yao, P., Wang, Z. B., Zhang, C. K., & Stive, M. J. F. (2017b). Exploratory morphodynamic modeling of the evolution of the Jiangsu coast, China, since 1855: Contributions of old Yellow River-derived sediment. *Marine Geology*, *390*, 306–320. https://doi.org/10.1016/j.margeo.2016.10.013

Sutherland, T. F., Amos, C. L., & Grant, J. (1998). The erosion threshold of biotic sediments: A comparison of methods. In K. S. Black, D. M. Paterson, & A. Cramp (Eds.), *Sedimentary progresses in the intertidal zone* (Vol. 139, pp. 295–307). London: Geological Society. https://doi.org/10.1144/gsl.sp.1998.139.01.24

te Slaa, S., He, Q., van Maren, D. S., & Winterwerp, J. C. (2013). Sedimentation processes in silt-rich sediment systems. *Ocean Dynamics*, *63*(4), 399–421. https://doi.org/10.1007/s10236-013-0600-x

te Slaa, S., van Maren, D., He, Q., & Winterwerp, J. (2015). Hindered settling of silt. *Journal of Hydraulic Engineering*, 04015020. https://doi.org/10.1061/(ASCE)HY.1943-7900.0001038

Thomas, N. (2000). Reverse and intermediate segregation of large beads in dry granular media. *Physical Review E*, *62*(1), 961–974. https://doi.org/10.1103/PhysRevE.62.961

van Ledden, M., van Kesteren, W. G. M., & Winterwerp, J. C. (2004). A conceptual framework for the erosion behavior of sand-mud mixtures. *Continental Shelf Research*, *24*(1), 1–11. https://doi.org/10.1016/j.csr.2003.09.002

van Rijn, L. C. (1993). *Principles of sediment transport in rivers, estuaries and coastal seas part 1* (Vol. 1006). Aqua Publications.

van Rijn, L. C. (2006). *Principles of sediment transport in rivers, estuaries and coastal seas part 2_supplement/update* (Vol. 1006). Amsterdam: Aqua publications.

van Rijn, L. C. (2007a). Unified view of sediment transport by currents and waves. I: Initiation of motion, bed roughness, and bed-load transport. *Journal of Hydraulic Engineering*, *133*(6), 649–667. https://doi.org/10.1061/(ASCE)0733-9429(2007)133:6(649)

van Rijn, L. C. (2007b). Unified view of sediment transport by currents and waves. III: Graded beds. *Journal of Hydraulic Engineering*, *133*(7), 761–775. https://doi.org/10.1061/(ASCE)0733-9429(2007)133:7(761)

van Rijn, L. C. (2020). Erodibility of mud-sand bed mixtures. *Journal of Hydraulic Engineering*, *146*(1), 04019050. https://doi.org/10.1061/(ASCE)HY.1943-7900.0001677

Wang, Y. N., Cai, H., Ma, H. J., & Sun, D. H. (2007). Research on real-time wireless sediment measurement system and its application in annular flume. *Ocean Engineering*, *25*(3), 132–135. (in Chinese with English Abstract).

White, S. J. (1970). Plane bed thresholds of fine grained sediments. *Nature*, *228*(5267), 152–153. https://doi.org/10.1038/228152a0

Winterwerp, J. C., & van Kesteren, W. G. (2004). *Introduction to the physics of cohesive sediment in the marine environment* (Vol. 56). Elsevier Science Limited.

Wu, W., Perera, C., Smith, J., & Sanchez, A. (2018). Critical shear stress for erosion of sand and mud mixtures. *Journal of Hydraulic Research*, *56*(1), 96–110. https://doi.org/10.1080/00221686.2017.1300195

Yao, P., Hu, Z., Su, M., Chen, Y., & Ou, S. (2018). Erosion behavior of sand-silt mixtures: The role of silt content. *Journal of Coastal Research*, *SI*(85), 1171–1175. https://doi.org/10.2112/SI85-235.1

Yao, P., Su, M., Wang, Z. B., van Rijn, L. C., Zhang, C. K., Chen, Y. P., & Stive, M. J. F. (2015). Experiment inspired numerical modeling of sediment concentration over sand-silt mixtures. *Coastal Engineering*, *105*, 75–89. https://doi.org/10.1016/j.coastaleng.2015.07.008

Yao, P., Sun, W., Guo, Q., & Su, M. (2022). Experimental study on the effect of sediment composition and water salinity on settling processes of quartz silt in still water. *Journal of Sediment Research*, *47*(5). (in Chinese with English Abstract).

Zhang, C. K. (Ed.). (2012). *The Comprehensive Survey and Evaluation Report on Coastal Zone of Jiangsu Province*. Beijing: Science Press.

Zhang, M., & Yu, G. (2017). Critical conditions of incipient motion of cohesive sediments. *Water Resources Research*, *53*(9), 7798–7815. https://doi.org/10.1002/2017WR021066